Europe PMC Funders Group
Author Manuscript
Nature. Author manuscript; available in PMC 2016 June 13.

Published in final edited form as:
Nature. 2015 July 16; 523(7560): 333–336. doi:10.1038/nature14461.

Supramolecular assemblies underpin turnover of outer membrane proteins in bacteria

Patrice Rassam[1,2], **Nikki A. Copeland**[2], **Oliver Birkholz**[3], **Csaba Tóth**[2], **Matthieu Chavent**[1], **Anna L. Duncan**[1], **Stephen J. Cross**[2], **Nicholas G. Housden**[1], **Renata Kaminska**[1], **Urban Seger**[2], **Diana M. Quinn**[2], **Tamsin J. Garrod**[2], **Mark S.P. Sansom**[1], **Jacob Piehler**[3], **Christoph G. Baumann**[2], and **Colin Kleanthous**[1]

[1]Department of Biochemistry, University of Oxford, South Parks Road, Oxford, OX1 3QU, UK

[2]Department of Biology, University of York, York, YO10 5DD, UK

[3]Department of Biology, University of Osnabrück, Barbarastraße 11, 49076 Osnabrück, Germany

Abstract

Gram-negative bacteria inhabit a broad range of ecological niches. For *Escherichia coli*, this includes river water as well as humans and animals where it can be both a commensal and a pathogen1–3. Intricate regulatory mechanisms ensure bacteria have the right complement of β-barrel outer membrane proteins (OMPs) to enable adaptation to a particular habitat4,5. Yet no mechanism is known for replacing OMPs in the outer membrane (OM), a biological enigma further confounded by the lack of an energy source and the high stability6 and abundance of OMPs5. Here, we uncover the process underpinning OMP turnover in *E. coli* and show it to be passive and binary in nature wherein old OMPs are displaced to the poles of growing cells as new OMPs take their place. Using fluorescent colicins as OMP-specific probes, in combination with ensemble and single-molecule fluorescence microscopy *in vivo* and *in vitro*, as well as molecular dynamics (MD) simulations, we established the mechanism for binary OMP partitioning. OMPs clustered to form islands of ~0.5 μm diameter where their diffusion was restricted by promiscuous interactions with other OMPs. OMP islands were distributed throughout the cell and contained the

Users may view, print, copy, and download text and data-mine the content in such documents, for the purposes of academic research, subject always to the full Conditions of use:http://www.nature.com/authors/editorial_policies/license.html#terms

Correspondence and requests for materials should be addressed to C.K. (colin.kleanthous@bioch.ox.ac.uk) and C.G.B. (christoph.baumann@york.ac.uk).
Present Addresses:
Nikki Copeland, 81 Furness Building, Faculty of Health & Medicine, Division of Biomedical and Life Sciences, Lancaster University, Lancaster LA1 4YQ, UK
Stephen J. Cross, School of Biochemistry, Medical Sciences Building, University Walk, Clifton, Bristol, BS8 1TD, UK
Tamsin J. Garrod, Basil Hetzel Institute, Adelaide University, Woodville Road, Adelaide, SA 5011, Australia
Csaba Tóth, Biomedica Slovakia s.r.o., Drobného 27, 841 01 Bratislava, Slovakia
Urban Seger, medi | Zentrum für medizinische Bildung, Max-Daetwyler-Platz 2, 3014 Bern, Switzerland

Author Contributions P.R., O.B., J.P., M.S.P.S., C.G.B. and C.K. designed the experiments. N.A.C., assisted by C.G.B. and C.T., collected SMT-TIRFM data and C.T., assisted by N.A.C. and P.R., collected FRAP data for colicin-labelled OMPs using wild-type and deletion *E. coli* strains. P.R. conducted all ensemble TIRFM experiments on OMP islands. U.S. and C.G.B. designed and built the TIRF microscope at York used for all SMT-TIRFM experiments. O.B. and P.R. conducted all PSM experiments and data analysis. S.J.C. and C.G.B. designed and implemented software scripts used for diffusion simulations and bacterial cell image analysis. C.T., P.R., N.A.C., N.G.H and R.K. purified all the proteins used in the study. C.T., P.R. and N.A.C. labelled colicins with fluorophores. D.M.Q. and T.J.G. constructed plasmids for colicin constructs and established procedures for growth of wild-type and gene deletion *E. coli* strains. M.C. and A.D. conducted the MD simulations and subsequent analysis. C.K. drafted the paper with assistance from P.R., C.G.B., M.S.P.S. and J.P.

Europe PMC Funders Author Manuscripts
Europe PMC Funders Author Manuscripts

Europe PMC Funders Author Manuscripts

Europe PMC Funders Author Manuscripts

Bam complex, which catalyses the insertion of OMPs in the OM7,8. However, OMP biogenesis occurred as a gradient that was highest at mid-cell but largely absent at cell poles. The cumulative effect is to push old OMP islands towards the poles of growing cells, leading to a binary distribution when cells divide. Hence the OM of a Gram-negative bacterium is a spatially and temporally organised structure and this organisation lies at the heart of how OMPs are turned over in the membrane.

We developed a strategy for following the localisation and turnover of OMPs using colicins, 9,10 which circumvents the need for fluorescent protein fusions. Protein fusions are the method-of-choice for investigating the localization of cytoplasmic, inner membrane and periplasmic proteins,11 but these generally inhibit OMP maturation. Colicins are species-specific bacteriocins that bind OMP receptors prior to translocating a cytotoxic domain into the cell9. ColE9 and Colla were used here as specific, high-affinity (~nM), non-covalent labels for the vitamin B_{12} transporter BtuB and the iron siderophore transporter Cir, respectively (Fig. 1a)12–14. The colicins were engineered with disulphide bonds to block their import into bacterial cells12 and covalently modified with organic fluorophores (Alexa Fluor^{488}, AF488, or tetramethyl rhodamine, TMR). We first compared the distribution and turnover of ColE9^{TMR} labelled BtuB in the OM with an inner membrane protein (IMP), GFP-labelled TatA, by confocal fluorescence microscopy (CFM) following simultaneous, pulsed production of both proteins. These experiments were carried out over several rounds of cell division using *E. coli* JM83 cells expressing *btuB* and *tatA-GFP*15 genes from arabinose-inducible promoters, in this instance using a variant of ColE9 ($\Delta^{1\text{-}83}$ ColE9^{TMR}) to label BtuB. Unlike TatA-GFP, which showed a purely analogue diminution of fluorescence in the inner membrane as cells divided, BtuB-ColE9^{TMR} distribution was binary in nature (Fig. 1b and f; Video 1). The OMP migrated towards the old poles during the first cell division and thereafter was sequestered predominantly in two cells, which we designated Repository Cells (RCs). RCs retained the bulk of the transiently-produced OMP (BtuB) leaving daughter cells to acquire new (unlabelled) OMPs. To ensure transient expression had not influenced OMP behaviour we repeated these experiments but this time observed endogenous BtuB and Cir migration in JM83 cells, following labelling with the respective colicin (Video 2). Starting from a single cell, the two OMPs behaved identically. Approximately half of each OMP moved toward the poles as the cell grew and divided and were then retained in two RCs while new daughter cells received little or no old colicin-labelled OMP.

We used a combination of laser scanning confocal fluorescence recovery after photobleaching (FRAP) and total internal reflection fluorescence microscopy (TIRFM) to determine the mechanistic basis of binary OMP partitioning in *E. coli*. Fluorescence recovery was rapid for TatA-GFP (<3 s at 37°C), which is typical of IMPs15, whereas no recovery was observed for colicin-labelled BtuB or Cir even after 3 min (Extended Data Fig. 1), similar to the OMP OmpA16. From single-molecule tracking (SMT)-TIRFM we established that BtuB and Cir have planar diffusion coefficients (D ~0.013 and 0.019 μm^2/s, respectively) similar to those reported previously for IMPs and OMPs *in vivo* (Extended Data Fig. 2a,b and Table 1; Videos 3 and 4) demonstrating that colicin-labelled OMPs diffuse in the membrane. However, mean square displacement (MSD) plots indicated this

Europe PMC Funders Author Manuscripts

Europe PMC Funders Author Manuscripts

diffusion was restricted to regions of ~0.5 μm diameter. Analysis of various *E. coli* mutants indicated that cell envelope structures such as cross-bridges to the peptidoglycan were not responsible for the restricted diffusion of OMPs (Extended Data Fig. 3 and Table 1). However, Monte Carlo simulations of BtuB diffusion were consistent with its confinement being due to an increase in mass over time, such as through association with other OMPs (Extended Data Fig. 2c), a point we return to below.

We next investigated the distribution and co-localisation of colicin-labelled BtuB and Cir in *E. coli* JM83 cells using TIRFM. BtuB-ColE9^{AF488} and Cir-Colla^{TMR} clustered together in islands that were distributed throughout the cell and moved to the poles as cells divided (Fig. 1c, d). Similar punctate appearance of trimeric porins in the OM of *E. coli* has previously been reported17,18. OMP islands contained multiple copies of BtuB and Cir (mean ~7; Extended Data Fig. 4a) and their mean size was ~0.5 μm (Fig. 1e), equivalent to the confinement diameter observed in SMT-TIRFM experiments. Linking these two observations we suggest restricted diffusion of OMPs in the OM reflects confinement within OMP islands. Taking the cross-sectional diameters of the BtuB and Cir β-barrels (~50 Å) as the average for an OMP, these data further suggest that a typical island comprises many hundreds of OMPs. Hence, OMP islands contain other OMPs not just BtuB and Cir.

Focusing on BtuB, we compared the behaviour of new and old OMPs in the OM. ColE9^{TMR} (*red*) and ColE9^{AF488} (*green*) were used to label old and new BtuB, respectively, where the addition of labels was staggered by a growth phase (Fig. 2 and Video 5). Temporal separation of the labels yielded poor or no co-localisation in both confocal and TIRF microscopy experiments. Old BtuB-containing islands accumulated at the poles of dividing cells while new OMP islands took their place. The new OMPs moved to the poles in the next division as they became old OMPs (Fig. 2a). Importantly, these data highlighted a gradient of OMP biogenesis that was greatest at mid-cell and diminished towards the poles (Fig. 2b). The movement of old OMP islands to the poles is the result of this asymmetric biosynthesis. The TIRFM data also demonstrated the stochastic nature of OMP biogenesis, with cell-to-cell variation in both number and distribution of new OMP islands.

OMPs are deposited in the OM of Gram-negative bacteria by the Bam machinery although where or how this occurs is not known7. We found that components of the Bam complex (BamA and BamC), which were labelled with fluorescently-labelled antibodies,19,20 showed significant co-localization with BtuB- and Cir-containing OMP islands and that this co-localisation persisted as islands migrated toward the poles (Fig. 3a,b and Extended Data Fig. 4b, c). Importantly, new Bam-containing islands appeared in non-polar regions of dividing cells consistent with these regions being the major sites of OMP biogenesis (Fig. 2b).

The co-localisation of different OMPs (BtuB, Cir, BamA) within islands and their restricted diffusion suggested promiscuous protein-protein interactions (PPIs) might be the underlying cause. To test this hypothesis we reconstituted BtuB in a polymer-supported membrane (PSM)21 prepared from an *E. coli* lipid extract and followed the lateral mobility of single molecules after labelling with ColE9^{TMR} (see Methods). At low BtuB densities (~50 BtuB/μm^2), similar to that estimated for the OM)22, the majority of BtuB-ColE9^{TMR} complexes

Europe PMC Funders Author Manuscripts

Europe PMC Funders Author Manuscripts

exhibited Brownian diffusion with trajectories that extended beyond those observed *in vivo* (Fig. 4a and b, panel 1; Video 6) and with faster diffusion coefficients ($D \sim 0.18\ \mu m^2/s$). Over time, however, BtuB molecules began to diffuse more slowly suggesting self-association (Fig. 4b, panel 2 and Extended Data Fig. 5a). This interpretation was confirmed by experiments where BtuB was added at a 1000-fold higher concentration (Fig. 4b, panel 3). Addition of the trimeric porin OmpF at concentrations found in the OM of *E. coli* (1000-fold above that of BtuB) resulted in most of the BtuB-ColE9^{TMR} complexes exhibiting restricted diffusion similar to that seen *in vivo* ($D \sim 0.02\ \mu m^2/s$ and confinement diameter ~0.4 μm, respectively; Fig. 4b, panel 4 and Extended Data Fig. 2d). Addition of maltose binding protein, which had been engineered with a single transmembrane helix (TM-MBP), to the PSM (Fig. 4b, panel 5; Extended Data Fig. 5b, d) or lipopolysaccharide (LPS) (Extended Data Fig. 5b, c) did not induce BtuB clustering, indicating this effect was not simply due to crowding or LPS association, but involved interactions between OMPs. Recent atomic force microscopy (AFM) data and MD simulations indicate OMPs can self-associate in membranes23–25. Using coarse-grained MD simulations of BtuB and OmpF/BtuB mixtures at high local concentration, we further showed that OMPs have a propensity to engage in both homologous and heterologous associations that slow their diffusion (Fig. 4c-e, Extended Data Fig. 6 and 7 and Table 2). Promiscuous OMP-OMP interactions were largely, but not exclusively, mediated by aromatic residues displayed from the surfaces of their β-barrels. In the case of BtuB the same set of residues mediated both homologous and heterologous interactions (Fig. 4e). We hypothesise that OMP islands are stabilised *in vivo* by such promiscuous PPIs.

In conclusion, we have shown that biogenesis and turnover of OMPs in the Gram-negative bacterium *E. coli* are inextricably linked processes (see model in Extended Data Fig. 8). The resulting binary partitioning of OMPs ensures they are turned over rapidly, but also means old OMPs persist in RCs which implies bacterial populations have ‘memory’ of past OMP biosynthesis. The accumulation of old OMPs in RCs could also be a factor in cellular ageing as well as providing a route for the presentation of proteins at cell poles.26,27 The co-localisation of the Bam biogenesis machinery with the OMPs it has deposited in the membrane points to a high level of cellular organisation and coordination in the OM that has hitherto been unsuspected. Bam substrates include LptD28, which inserts LPS into the outer leaflet of the OM, and the β-barrels of autotransporters29 that are critical for biofilm formation and adhesion to host epithelia during bacterial pathogenesis. Moreover, since Bam is also required for the surface exposure of the OM lipoprotein RcsF through the pores of OMPs30, OMP and lipoprotein biogenesis may intersect within OMP islands.

Methods

Confirmation of single gene deletions in Keio collection strains

All Keio mutants31 of *E. coli* BW25113 used in this work (with deletions in *lpp*, *ompA*, *pal*, *rfaC*, *tolA* and *tonB*) were first validated by PCR, confirming the deletion strains contained the kanamycin resistance cassette within the ORF of interest.

Europe PMC Funders Author Manuscripts

Europe PMC Funders Author Manuscripts

Colicin purification and fluorophore-labelling

Site-directed mutagenesis was used to introduce a solvent accessible cysteine (K469C) in the cytotoxic domain of a disulphide inactivated (Y324C, L447C) ColE9·$Im9_{His6}$ construct, cloned into pET-21a32. An equivalent Y324C, L447C, K469C ColE9 construct in which the N-terminal 83 amino acids of the colicin had been deleted (Δ^{1-83} ColE9) was also generated. This intrinsically disordered region of the colicin contains important protein-protein interaction epitopes that are required for translocation into the cell10. Removal of this region had no impact on the localisation of OMP islands or on the turnover of OMPs. It was used primarily during long time courses where reduction of the inactivating disulphide bond was possible.

Standard recombinant molecular biology techniques were used to clone the *colla* gene into pET-21a with a C-terminal His_6-tag and to introduce an inactivating disulphide within the coiled-coil R-domain (L257C, A411C), analogous to that used to inactivate ColE9, in addition to a solvent exposed cysteine in the cytotoxic domain (K544C).

All recombinant proteins were expressed in *E. coli* BL21 (DE3) cells and purified by nickel affinity and size exclusion chromatography using published procedures33. Elution from the nickel affinity column was achieved through guanidine denaturation of the ColE9-$Im9_{His6}$ complex and imidazole elution of $Colla_{His6}$.

Cys469 and Cys544 within ColE9 and Colla, respectively, were labelled with a 20-fold molar excess of fluorophore (AlexaFluor 488-maleimide (Invitrogen) or TMR-maleimide (Sigma) in 20 mM potassium phosphate, pH 7.0, 2 M guanidine-HCl for 30 min at 37°C followed by dialysis against 20 mM potassium phosphate, pH 7.0, 0.5 M NaCl at 4°C. Dialysed proteins were further purified by size-exclusion chromatography (Superdex S200 HR 10/30, GE Healthcare) performed in the same buffer at room temperature and fractions containing fluorescently-labelled protein analysed by SDS-PAGE, pooled, snap frozen and stored in aliquots at -20°C. All labelling and subsequent purification steps were performed in the dark. The labelling efficiency (typically > 0.7 fluorophores/protein) was estimated from the spectrophotometrically determined fluorophore (Alexa Fluor 488, ε_{max} = 71,000 $cm^{-1}M^{-1}$; TMR, ε_{max} = 80,000 $cm^{-1}M^{-1}$) and colicin (ColE9, ε_{280} = 46,075 $cm^{-1}M^{-1}$; Colla, ε_{280} = 59,360 $cm^{-1}M^{-1}$) concentrations after correcting for absorption at 280 nm by the fluorophore (Alexa Fluor 488, $A_{280} = 0.11*A_{495}$; TMR, $A_{280} = 0.3*A_{547}$). Analysis of single-molecule photobleaching characteristics for fluorophore-labelled colicins adsorbed on a quartz slide surface and viewed by TIRFM were consistent with labelling at a single position.

Membrane protein purification

OmpF and BtuB were purified according to previously published protocols10,12. The purified proteins contained some endogenous LPS carried through the purification.An artificial transmembrane domain (ALAALAALAALAALAALAALAKSSR) was fused to the C-terminus of maltose-binding protein (TM-MBP) by insertion of the corresponding oligonucleotide linker into the MCS of pMALc2x via restriction with *BamH*I and *Hind*III34. For efficient purification and fluorescent labelling, an N-terminal His_{10}-tag and a ybbR-tag

Europe PMC Funders Author Manuscripts

Europe PMC Funders Author Manuscripts

(DSLEFIASKLA)35 were inserted via the *Nde*I site. This protein was expressed in *E. coli* TG-1 cells at 37 C according to standard protocols. After cell lysis, the membrane fraction was solubilized with buffer containing 20 mM Triton X-100 and the protein purified by immobilized metal ion affinity chromatography (5 ml HiTrap Chelating, GE Healthcare). The protein was then covalently modified using a 2-fold molar excess of Coenzyme A-Dy647 in the presence of 5 μM of the phosphopantetheinyl transferase Sfp and 10 mM Mg^{2+} for 1 h at room temperature35. Finally, labelled TM-MBP (TM-MBP^{Dy647}) was further purified by size exclusion chromatography in 20 mM Hepes, 150 mM NaCl pH 7.5 containing 0.6 mM Triton X-100 (Superdex 200 10/300 GL, GE Healthcare).

Cell growth and OMP staining with colicins and antibodies

E. coli JM83 cells were grown at 37°C in LB broth to exponential phase, upon which 200 μl of cells were transferred to 4 ml M9-glucose minimal media (0.1 mM $CaCl_2$, 0.1 mM $FeSO_4$, 2 mM $MgSO_4$, 1 g/l NH_4Cl, 0.05% w/v casamino acids, 0.0002% w/v thiamine, 0.4% w/v D-glucose) and grown until OD_{600}~0.4. 200 μl of cells were pelleted by centrifugation (4,700 x g, 3 min) with the pellet resuspended in 200 μl of fresh supplemented M9-glucose containing 300 nM fluorescently labelled colicin. After 15 min incubation at room temperature with mixing by rotary inversion, cells were washed twice by pelleting (4,700 x g, 3 min) and resuspended in 500 μl fresh M9-glucose, before finally resuspending the pellet in 100 μl supplemented M9-glucose. For sequential labelling of old and new OMPs, cells were grown for a further hour after the initial labelling such that the OD_{600} had approximately doubled before a second staining was performed. Wash steps were repeated as above. For the transient expression of BtuB10 and TatA-GFP36 from pBAD plasmids, cultures were grown in the presence of 100 μg/ml ampicillin, and 0.2 mM L-arabinose added for 1 h prior to cells being used in confocal experiments.

For detection of BamA, JWD3 cells transformed with a pET17b plasmid expressing BamA-HA-L7 were grown in the presence of 100 μg/ml ampicillin and 50 μg/ml kanamycin, and prepared for microscopy as described for JM83 cells above. Browning et al.19 have shown that insertion of an HA epitope into loop 7 of BamA is tolerated functionally and exposed on the external surface of bacteria. BamA-HA-L7 was labelled *in vivo*, adding a 1:500 dilution of $Alexa^{488}$-anti-HA antibody (Molecular Probes®) and 1% (w/v) ultrapure BSA (Invitrogen) to 100 μl of JWD3 cells. After 15 min incubation with mixing by rotary inversion at room temperature, excess label was removed as described above for colicins.

For BamC labelling, a 1:1000 dilution of mouse anti-BamC antibody20 (gift of Susan Buchanan, NIH) was added to 100 μl of JM83 cells prepared as above in the presence of 2% (w/v) ultrapure BSA and incubated for 15 minutes with mixing by rotary inversion at room temperature. Cells were then washed twice by pelleting (4,700 x g, 3 min) and resuspended in 500 μl of fresh supplemented M9 media, before a 1:500 dilution of $Alexa^{488}$-anti-mouse secondary antibody (Molecular Probes) was added in the presence of 2% (w/v) ultrapure BSA. After 15 min incubation with rotary inversion at room temperature excess label was removed as described above for colicins. For sequential labelling of old OMPs and new BamC, old BamC was first blocked with mouse anti-BamC antibody and unlabelled anti-mouse secondary antibody, as described above, while old BtuB or old Cir were stained with

Europe PMC Funders Author Manuscripts

Europe PMC Funders Author Manuscripts

ColE9^{TMR} or Colla^{TMR}, respectively. After 1 h of growth at 37°C in M9-glucose media, where the OD_{600} had approximately doubled, new BamC was then labelled with mouse anti-BamC antibody and Alexa^{488}-anti-mouse secondary antibody, implementing the same wash steps described above.

FRAP microscopy

25 μl of stained *E. coli* cells were immobilised on poly-D-lysine (30-70 kDa, Sigma) coated coverslips and then imaged for less than one hour at 20 or 37°C. Cell viability under identical experimental conditions was verified using the LIVE/DEAD BacLight bacterial viability kit (Molecular Probes). Measurements were made using a Zeiss laser-scanning confocal microscope (LSM 510 Meta or LSM 710 Meta/Axiovert 200M) equipped with 30 mW Ar ion and 1 mW HeNe lasers. Optical magnification was provided by a 63x oil-immersion objective (Zeiss, NA 1.4). Bleaching of fluorescently-labelled proteins was performed using 20 (488 nm laser) or 500 (543 nm laser) scan iterations (1.58 μsec pixel dwell time) over a rectangular ROI with a 10x digital zoom and the laser power set to 50-100% (depending on laser line). To minimise photobleaching, FRAP was monitored using reduced laser power (2-10% depending on laser line). The diameter of the pinhole was varied between 0.2-0.3 μm depending on the sample conditions and the fluorophore used. Two-colour FRAP experiments (GFP and TMR) on a single bacterial cell were performed as follows: (1) acquire pre-bleach and first post-bleach image with 543 nm laser illumination, (2) record complete FRAP sequence for TatA-GFP with 488 nm laser illumination, and (3) record post-bleach images with 543 nm laser illumination. The individual laser sources were used separately to prevent cross-talk between the two fluorescence emission channels. A differential interference contrast (DIC) microscopy image was acquired before and after each FRAP experiment to ensure the image of the bacterial cell remained in focus and adherent to the PDL coated surface. In all cases, DIC images were recorded using a 633 nm laser to prevent photobleaching of fluorescent probes.

In vivo single molecule tracking (SMT)-TIRF microscopy

JM83 cells were immobilised on poly-D-lysine coated quartz slides (25 mm x 75 mm, cleaned in 1 M KOH) in supplemented M9 media containing 100 nM fluorescently-labelled colicin. An ultra-thin sample chamber was formed by adding ~0.1 μg/ml of 5 μm silica beads to the media, overlaying with a no. 1 coverslip (22 mm x 64 mm) and sealing with nail varnish. An inverted Zeiss IM35 microscope chassis fitted with a 100x oil-immersion objective (Zeiss Plan-Apochromat, NA 1.4) was modified in-house for prism-coupled TIRFM. Illumination was provided by 488 nm (30 mW) and 561 nm (30 mW) optically-pumped solid-state lasers (Sapphire LP, Coherent). A λ/4 waveplate was used to depolarise the laser excitation, thus ensuring fluorophore orientation effects were minimised. The fluorescence image was separated into two channels using an image splitter (Optosplit II, Cairn Research) with appropriate dichroic beamsplitter (FT580, Zeiss) and band pass filters for Alexa Fluor 488 (ET525/50M, Chroma) and TMR (HQ605/20M, Chroma). Background datasets were obtained by directly adsorbing fluorescently-labelled colicins to poly-D-lysine coated quartz slides. Moderate photobleaching of each sample was done to enable detection and tracking of single fluorophores. Analogue video (IC-300B intensified CCD, Photon Technology International) was recorded at 30 fps (494 pixels x 786 pixels) and digital video

Europe PMC Funders Author Manuscripts

Europe PMC Funders Author Manuscripts

(DU897E emCCD, Andor; Evolve 512 emCCD, Photometrics) was recorded at 30 fps (512 pixels x 512 pixels) or 58 fps (128 pixels x 128 pixels). All video data was collected at room temperature (20-22°C). In analogue video data, single fluorophores were identified manually and tracked using GMimPro software37. In digital video data, single fluorophores were identified automatically (using standard FWHM and threshold values) and tracked using the automated SPT function in GMimPro. *D* values were extracted from the time-dependence of the mean-square displacement (MSD) using either linear regression or power law fitting of the initial 4-5 time delays. The confinement diameter (d) was calculated according to the equation: $A = (d/2)^2/6$, where A is the asymptotic MSD value38.

Monte Carlo simulations of two-dimensional diffusion

MATLAB was used to model diffusion in the *E. coli* outer membrane (OM) using a standard Monte Carlo approach38. At each time point (dt), a diffusion step (dl) with length $(4Ddt)^{-1/2}$, where *D* is the diffusion coefficient, was taken in a uniformly-distributed random direction39,40. All simulations were performed for 5000 particles, over a total simulation time (t) of 2 s at intervals dt = 1 μs, unless otherwise stated. Particle runs were performed sequentially; therefore, to reduce computational overheads, the cumulative moving mean $(\overline{x}_n)$ and variance $\left(\sigma_n^2\right)$ of the MSD were calculated following each particle run, where n is the current iteration:

$$\overline{x}_n = \frac{\left(\sum_{i=1}^{n-1} x_i + x_n\right)}{n}$$

$$\sigma_n^2 = \frac{(n-1)\sigma_{n-1}^2 + (\overline{x}_n - \overline{x}_{n-1})(x_n - \overline{x}_n)}{n}$$

Curvature of the cellular membrane was modelled by mapping planar diffusion coordinates onto a hemispherically-capped cylinder of length 3 μm and radius 250 nm. The limited TIRF evanescent field depth was modelled by terminating, but not discarding, particle paths which diffused further than 150 nm from the closest observable plane.

Molecular crowding in the OM was simulated using excluded volume of BtuB and two of the most abundant proteins in the OM, OmpA and OmpF. Each protein species was modelled in 2D as a series of single, non-overlapping, hard circles with radii of R_{OmpA} = 1.3 nm, R_{OmpF} = 3.1 nm and R_{BtuB} = 2.3 nm, and with relative populations of 333, 111 and 1, respectively. A random planar distribution of OmpA and OmpF was generated for each diffusing BtuB up to the percentage membrane occupancy, δ. BtuBs were randomly positioned and subject to the standard Monte Carlo-based diffusion approach; however, only steps ending in vacant positions (no overlap of BtuB with OmpA or OmpF) were accepted. To model association of BtuB with the OmpF population in the OM, the BtuB radius was increased randomly in a single step according to the following equation and association rate, k.

$$R_{BtuB+OmpF} = \sqrt{R_{BtuB}^2 + R_{OmpF}^2}$$

Planar diffusion trajectories were subsequently mapped to the curved bacterial surface as described previously. For optimisation of the MSD simulated under molecular crowding conditions, the rate k and parameters D (= 0.01-0.3 μm^2/s) and δ (≤ 20%) were varied manually. Very similar parameters to those for OmpF-BtuB association were generated for OmpA-BtuB association, thus only those for OmpF are shown in Extended Data Fig. 2c. Monte Carlo simulations that did not include promiscuous association between OMPs, but merely membrane crowding ($\delta \leq 20\%$), did not reproduce the *in vivo* diffusive behaviour (data not shown), which is consistent with an increase in mass of the tracked diffusing species explaining the asymptotic experimental MSD observed *in vivo* and *in vitro*.

Analysis of OMP islands by TIRF microscopy

JM83 cells were immobilised on poly-D-lysine and viewed using prism-coupled TIRFM as described above. 100 consecutive video frames were stacked to build an image that was then analysed. Only sequences with no saturation of the intensified CCD camera were selected. For each picture and each channel, we used ImageJ41 software to select only pixels that were 3 times more intense than background for further quantification. Intensity quantification within individual spots was obtained using ImageJ. Within each cluster or island, the total pixel intensity was normalised so the population corresponding to a single photobleaching step was fitted to 1 AU.

CoLocalizer Pro 2.7.1 software (CoLocalization Research Software, www.colocalizer.com)42 was used for co-localisation of red and green channels. The co-localisation value corresponded to the ratio between yellow pixels over the sum of yellow, red and green pixels on each overlapped picture. Distribution of fluorescence intensity along the x-axis of bacteria was determined using a custom script implemented in MATLAB (version 2012a, MathWorks, Cambridge, UK). Raw images were initially thresholded against a user-defined intensity (selection via GUI) to provide a binary image, approximately highlighting bacteria against the background. High frequency noise was reduced through application of the built-in MATLAB medfilt2 median filter. Individual bacteria were identified as continuous high intensity pixel regions, with pixels of a continuous region required to be within a 0.6 μm^2 area of each other. Further filtering was performed to remove bacteria less than 1 μm away from their neighbour to improve the quality of intensity profile analysis results. Bacterial poles were identified as corresponding to the two pixels in a continuous region with the largest separation. Intensity along the selected bacteria was measured 11 times between the bacterial end-points, each at a uniformly-spaced offset from the bacterial long axis in the range +/- 200 nm. The mean profile is calculated and normalised to the range 0-100 for comparison between bacteria.

Confocal time-lapse microscopy

200 μl of M9 containing 1% agarose (w/v) was introduced into a Gene Frame® matrix that was previously adhered to a clean slide. The agar pad was formed by addition of a clean

Europe PMC Funders Author Manuscripts
Europe PMC Funders Author Manuscripts

Europe PMC Funders Author Manuscripts

Europe PMC Funders Author Manuscripts

coverslip on top until solidification had occurred. 10 μl of stained bacteria were then added to the pad, which was sealed afterward using a clean coverslip. Cell growth was monitored at 37°C and visualised through 100x oil-immersion objective (Zeiss Plan-APOCHROMAT NA 1.4) on a Zeiss LSM780 microscope. Individual cells were selected in a region of interest that was clear of other cells. Snapshots were taken every 30 minutes during 2-3 h time courses, using scan speed 7 and 1-2% of laser power (depending on laser line).

Formation of polymer-supported membranes

Modification of glass coverslips was performed as described previously34. In brief, surfaces were first cleaned by plasma cleaning and then activated by silanization with pure (3-Glycidyloxypropyl) trimethoxysilane (Sigma) at 75°C for 1 h. Subsequently, the surfaces were reacted with molten bis-amino-poly ethylene glycol (PEG) with a molecular mass of 2,000 Da (Rapp Polymere) for 4 h at 75°C. Modification of the free amines with palmitic acid (Sigma) was carried out in the presence of an excess of diisopropylcarbodiimide (Sigma). Formation of proteoliposomes was carried out by detergent extraction in lipid-protein-detergent mixtures by addition of β-cyclodextrin43. Lipids, proteins and lipopolysaccharides solubilized in Triton-X-100 or n-octyl-β-D-glucoside were combined as required before a two-fold excess of Heptakis(2,6-di-O-methyl)-β-cyclodextrin (Sigma) over the detergent was added. Reconstitution of BtuB was achieved by mixing an *E. coli* lipid extract with the protein in MES buffer pH6.5 and adding a two-fold molar excess of β-cyclodextrin. Experiments were conducted using either a defined *E. coli* polar lipid extract (PE 67%; PG 23.2%; CA 9.8%) or total *E. coli* lipid extract (PE 57.5%; PG 15.1%; CA 9.8%; unknown 17.6%) from Avanti Lipids. OMP mobilities in PSM experiments were essentially identical using these lipid extracts. So as to obtain a 1x final concentration of protein, a molar ratio of 1:100000 (protein:lipid) was prepared and vortexed for 2 s prior to deposition on surfaces. After 10 min the proteoliposomes were added onto functionalized surfaces and incubated for 20 min for immobilization. The buffer was then exchanged for a solution of 10% (w/v) PEG with a molecular weight of 8,000 Da (Sigma Aldrich, Germany) in order to induce fusion of the proteoliposomes into a homogenous lipid bilayer. After 20 min, the surfaces were extensively washed with buffer to remove excess vesicles. Before imaging, bilayer continuity was visualised by monitoring the homogeneous lateral diffusion of the lipids DiD^{Dy647} or LPS^{BODIPY} in the membrane. Prior to data acquisition, BtuB was labelled by the addition of 100 nM $ColE9^{TMR}$ for 5 min, followed by removal of unbound ligand. Assuming all BtuB molecules were labelled, and single step photobleaching corresponded to single molecules, the density of BtuB at 1x concentration was comparable to that estimated *in vivo* (~50 molecules/μm^2).

Tracking single molecules in polymer supported bilayers

OMPs were tracked using TIRF microscopy carried out with an Olympus IX71 inverted microscope equipped with a quad-line total internal reflection illumination (TIR) condenser (Olympus), a 150x magnification objective with a numerical aperture of 1.45 (UAPO 150x/1.45 TIRFM, Olympus) and a back-illuminated emCCD camera (Andor iXon Ultra 897). TMR was illuminated by a 561 nm diode-pumped solid-state laser (Cobold Jive, 200 mW) with 2 mW output power at the objective, whereas BODIPY and Dy647 were illuminated with 488 and 642 nm laser diodes (Omicron, 140 and 200 mW, respectively) with output

Europe PMC Funders Author Manuscripts

Europe PMC Funders Author Manuscripts

powers of 5 and 4 mW, respectively. Fluorescence was detected using a quadband emission filter (446/523/600/677 HC Quadband Filter, Semrock) with a time-resolution of 33 Hz. All experiments were carried out using buffer complemented with oxygen scavenger and a redox-active photoprotectant [0.5 mg/ml glucose oxidase (Sigma), 0.04 mg/ml catalase (Roche Applied Science), 5% glucose (w/v), 1 μM ascorbic acid and 1μM methyl viologene] to minimize photobleaching44. Moderate bleaching of the sample was applied to be able to track single molecules.

All videos were analyzed using custom software (PATRACK), implemented in visual C++ and provided by Pierre-Emmanuel Milhiet and Patrice Dosset (Montpellier, France). The centre of each fluorescence peak was determined with sub-pixel resolution by fitting a two-dimensional elliptical Gaussian function. The two-dimensional trajectories of single molecules were constructed frame-by-frame, selecting particles that displayed a single bleaching step. Diffusion coefficient values were determined from a linear fit to the MSD plots between the first and fourth points according to the equation: $MSD(t) = 4Dt$.

We used a new algorithm within PATRACK based on a back-propagation neural network allowing automatic detection of Brownian, confined and directed motion modes within a trajectory. The ability of the software to accurately detect different diffusion modes was first established on simulated data and then evaluated on trajectories recorded from fluorescently labelled molecules in two different biological systems45,46.

Statistical analysis of microscopy data

All experiments were conducted at least twice (no significant differences were observed between datasets either by student T-test or non-parametric Mann-Whitney test) and in each case a representative set of data presented in the figures. Sampling sizes in experiments (cells, OMP islands, single molecule trajectories) were validated by very significant p values in a student T-test or a non-parametric Mann-Whitney test. In the analysis of OMP islands in post growth conditions by TIRFM, cells that were undergoing division were explicitly selected for imaging.

MD simulations

Simulations were run using GROMACS (version 4) (www.gromacs.org) using a modified version of the MARTINI forcefield47–49. Structures of OmpF (2OMF) and BtuB (2GUF) were converted to coarse-grained models as described previously49. In the model, each coarse-grained particle represents approximately four atoms in the atomistic structure. Protein molecules were represented with a single coarse-grained particle per backbone moiety, with variable numbers of sidechain particles. To maintain the β-barrel structure of OmpF and BtuB, an elastic network model was used, with a force constant 1000 kJ mol^{-1} nm^{-2} applied between Cα particles within 7 Å of one another.

In order to mimic varied levels of crowding in the membrane, several systems of varying size and protein content were constructed (see Extended Data Fig. 6). Proteins were inserted into a pre-equilibrated bilayer containing POPE and POPG in a 3:1 ratio. The lipid composition was selected to approximate that used in PSM experiments. Using a membrane patch of ~ 30 x 30 x 10 nm^3, one of the following protein groups was inserted: a single

Europe PMC Funders Author Manuscripts

Europe PMC Funders Author Manuscripts

OmpF trimer; a single BtuB molecule; two OmpF trimers and two BtuB monomers or 4 BtuB monomers; four OmpF and five BtuB or 9 BtuB monomers; or eight OmpF and eight BtuB. Into a larger membrane patch of ~ 60 x 60 x 10 nm^3 were inserted: eight OmpF and eight BtuB; or 18 OmpF and 18 BtuB or 36 BtuBs (see Fig. 4c and Extended Data Fig. 6 to see final snapshots of the systems). Large systems were simulated in order to identify how system size might influence results, since differences have previously been observed50. In each case, OmpF and BtuB molecules were positioned on a square grid in an alternating pattern. To ensure no protein interaction face was favored in the starting configuration we randomized the rotation of each protein around its center of mass about the membrane normal. Systems were solvated and sodium counter ions were added to neutralize the system. Each system was equilibrated for 100 ns with the proteins restrained in the X-Y plane, using a force constant of 1000 kJ mol^{-1} nm^{-2}. Simulations were performed using a time step of 20 fs. A temperature of 313 K was maintained using the Berendsen thermostat, and coupled separately for proteins, lipids, and solvent. Pressure was maintained at 1 bar with a semi-isotropic coupling and using the Berendsen barostat, with a compressibility of 5 x 10^{-6} bar^{-1}. Electrostatic interactions were shifted between 0.0 and 1.2 nm, and Lennard-Jones interactions were shifted between 0.9 and 1.2 nm. Production runs, with no restraints applied, were for 10 μs (see Extended Data Fig. 6).

MD simulations analysis

Analysis was performed using in house scripts, MDAnalysis51, and VMD52.

Protein diffusion—Protein diffusion coefficients were calculated using an in-house python script (http://dx.doi.org/10.5281/zenodo.11827). Briefly, MSD was calculated for time windows between 1 ns and 10 % of the full simulation time (i.e. 10 μs), to allow for suitably sampled windows. Parameters were obtained by a linear fit to the MSD vs. time data, with error estimated as the difference in the slopes of the two halves of the data.

Interaction frequencies—In order to quantify interactions occurring during the simulations, we first define an interaction count function, $C_{\sigma,t}\left(res_{i,p1}, res_{j,p2}\right)$, to perform a simple count of the interactions between residues *i* and *j* of protein p_1 and p_2, respectively, at time *t* in simulation σ:

$$C_{\sigma,t}\left(res_{i,p1}, res_{j,p2}\right) = \begin{cases} 1 \text{ if the centroids of } res_i \text{ and } res_j \text{ are within 8 Å of each other} \\ 0 \text{ otherwise} \end{cases}$$

Thus, the interaction frequency, $int(res_i, res_j)$, between any two residues, res_i in BtuB and res_j in OmpF, is given by:

$$\text{int}(res_i, res_j) = \sum_{\sigma=1}^{N_{sims}} \sum_{t=T-100}^{T} \sum_{p_1=1}^{N_{BtuB,\sigma}} \sum_{p_2=1}^{N_{OmpF,\sigma}} C_{\sigma,t}\left(res_{i,p1}, res_{j,p2}\right)$$

where N_{sims} is the total number of simulations being considered; T is the total simulation time (in ns); and $N_{BtuB,\sigma}$ and $N_{OmpF,\sigma}$ are the total number of BtuB and OmpF proteins, respectively, in simulation σ. Only the last 100 ns of each simulation was used. The

Europe PMC Funders Author Manuscripts

Europe PMC Funders Author Manuscripts

proportional interaction frequency, $I_{i,j}$, is then given by normalising the interaction frequency for any pair of residues, $int(res_i,res_j)$, by the total number of interactions:

$$I_{i,j}=\frac{\mathrm{int}(res_i,res_j)}{\sum_{i=1}^{N_{res\ BtuB}}\sum_{j=1}^{N_{res\ OmpF}}\mathrm{int}(res_i,res_j)}$$

where $N_{res\ BtuB}$ and $N_{res\ OmpF}$ denote the number of residues in a BtuB and OmpF single protein, respectively.

In order to look at interactions of BtuB with itself, $int(res_i,res_j)$ is instead defined by:

$$\mathrm{int}\,(res_i,res_j)=\sum_{\sigma=1}^{N_{sims}}\sum_{t=T-100}^{T}\sum_{p_1=1,p_1\neq p_2}^{N_{BtuB,\sigma}}\sum_{p_2=1}^{N_{BtuB,\sigma}}\frac{1}{2}C_{\sigma,t}\,(res_{i,p1},res_{j,p2})$$

The factor of one half accounts for each interaction being counted twice. Similar to BtuB-OmpF interactions, $int(res_i,res_j)$ is normalised by the total number of interactions to give the proportional interaction frequency, $I_{i,j}$ for any two residues, res_i and res_j, on different monomers of BtuB. The proportional interaction frequency, I_i of a single residue, res_i, of BtuB with OmpF - the values shown in red bars on the side of the interaction frequency matrix plots (Extended Data Fig. 7) - is then given by summing the proportional interaction frequencies of res_i over all residues of OmpF:

$$I_j=\sum_{j=1}^{N_{res\ OmpF}}I_{i,j}=\frac{\sum_{j=1}^{N_{res\ OmpF}}\mathrm{int}\,(res_i,res_j)}{\sum_{i=1}^{N_{res\ BtuB}}\sum_{j=1}^{N_{res\ OmpF}}\mathrm{int}\,(res_i,res_j)}$$

Similarly, a single residue function is defined for the proportional interaction frequencies of OmpF with BtuB, and residues of BtuB in their interaction with other BtuB monomers.

Amino acid interaction propensities—In order to assess the involvement of each amino acid in mediating BtuB-OmpF and BtuB-BtuB interactions, a residue interaction propensity is defined, adapted from the residue propensity metric defined by Jones *et al.*53 in their hallmark work on protein-protein interactions. For each amino acid, AA_k, the interaction propensity, IP_{AA_k}, for the interaction of residues of BtuB with OmpF is given by comparing the proportion of BtuB interactions mediated by amino acid AA_k with the proportion of the BtuB surface it represents:

$$IP_{AA_k}=\frac{(\sum_{i=AA_k}I_i)/(\sum_{i=1}^{N_{res\ BtuB}}I_i)}{N_{AA_k,BtuBsurf}/N_{res_{BtuBsurf}}}$$

where $N_{AA_k,BtuBsurf}$ is the number of amino acid AA_k on the surface of BtuB, and $N_{res_{BtuBsurf}}$ is the total number of residues on the surface of BtuB. Similarly, residue

interaction propensities are defined for the OmpF interaction with BtuB and interaction of BtuB with other monomers of BtuB.

Extended Data

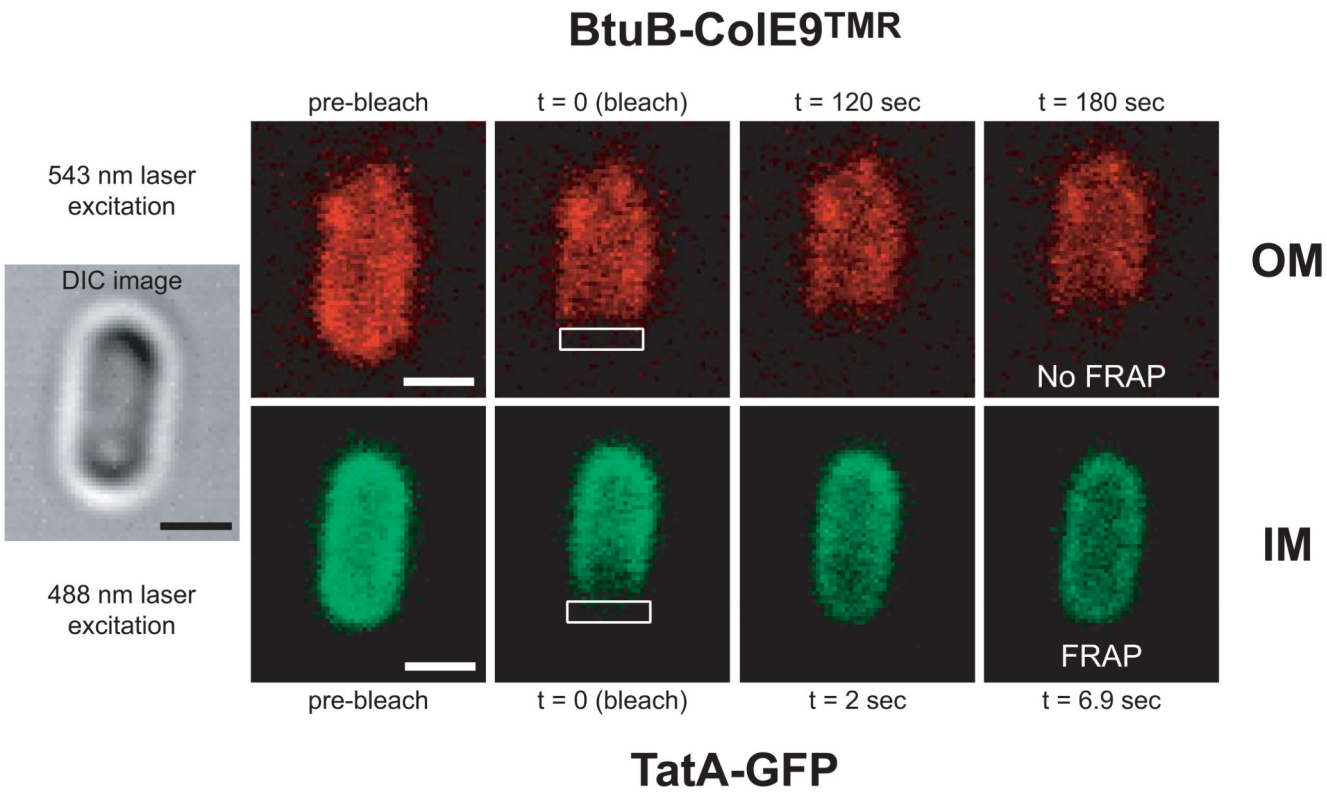

Figure 1. Visualising the different diffusive behaviours of proteins in the inner and outer membranes of the same *E. coli* cell.

Single *E. coli* JM83 bacterial cell visualised by laser-scanning confocal fluorescence microscopy at 37°C. At the OM (top row) BtuB-labelled with ColE9^{TMR} showed no fluorescence recovery after photobleaching a region of interest with a 543 nm laser (rectangle). In contrast, recovery of TatA-GFP fluorescence in the IM of the same cell (bottom row) was observed within a few seconds after photobleaching an identical region with 488 nm laser. The unrestricted mobility of TatA-GFP in the IM accounts for its analogue distribution during cell division (main text, Fig. 1b, f). This experiment was done in duplicate (one representative set of images is presented in the figure). Scale bar = 1 μm.

Europe PMC Funders Author Manuscripts
Europe PMC Funders Author Manuscripts

Europe PMC Funders Author Manuscripts

Europe PMC Funders Author Manuscripts

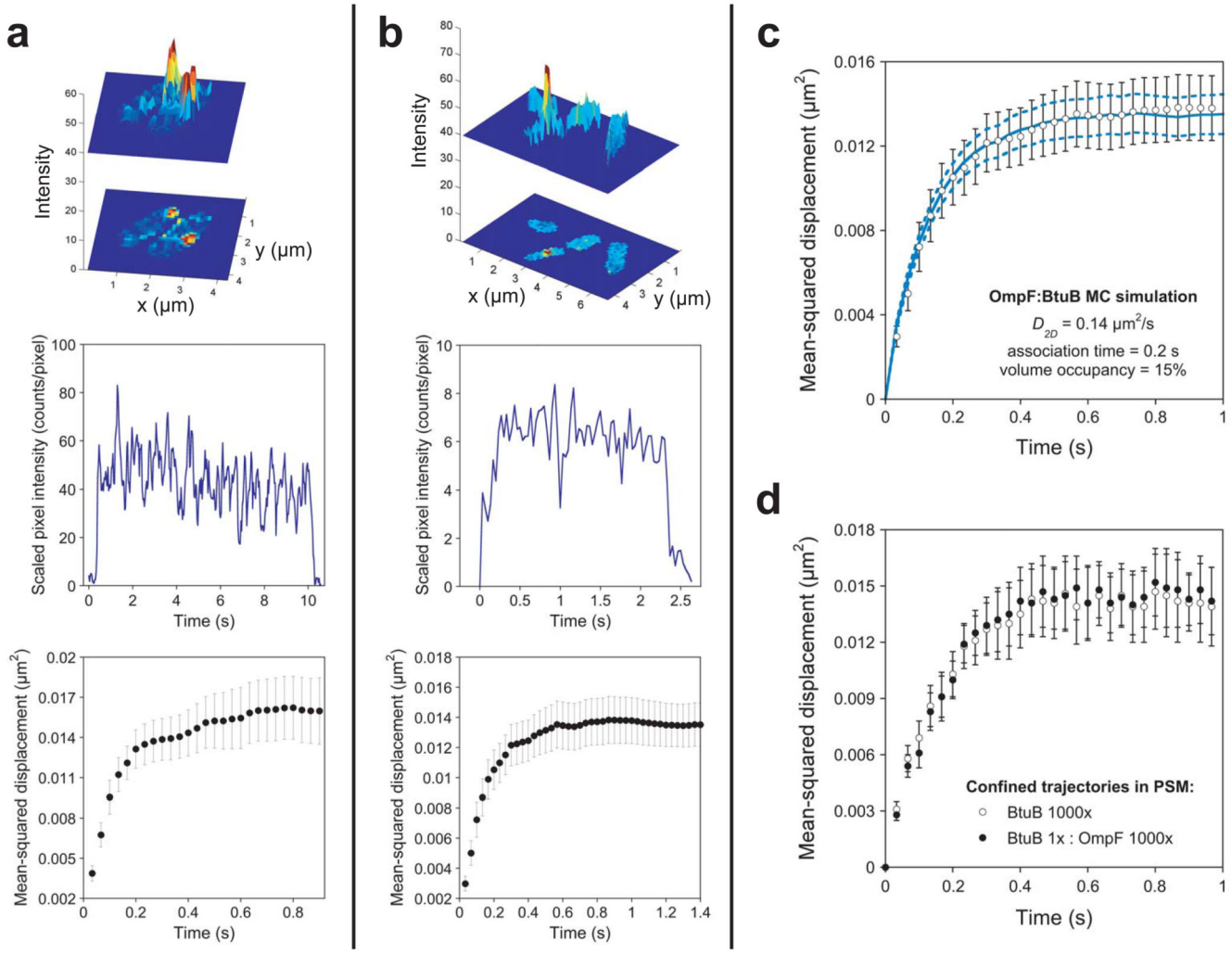

Figure 2. Single molecule tracking (SMT)-TIRFM defines the mobility of colicin-labelled BtuB and Cir *in vivo*.

a, *Top panel,* Z-projection of fluorescence intensity (increasing from blue to red) of two Cir-Colla^{AF488} complexes on separate JM83 cells. *Middle panel,* the fluorescence intensity in consecutive images (30 fps) is displayed for a typical Cir-Colla^{AF488} fluorescent spot. The intensity and single-step photobleaching behaviour were consistent with a single membrane complex being tracked. *Bottom panel,* mean squared displacement (MSD) was calculated for single Cir-Colla^{AF488} complexes ($N = 41$) that displayed single-step photobleaching behaviour, could be tracked for at least 1.7 s prior to photobleaching (error is reported as SEM) and were not immobilised on the quartz surface ($MSD_{end\ of\ trajectory} > 0.004$, determined for surface bound Colla^{AF488} in the same samples). The MSD value rapidly approached an asymptotic value that was consistent with restricted lateral diffusion. Linear regression of the MSD for the first 4 time delays (0.033-0.13 s) yielded the planar diffusion coefficient ($D \sim 0.019$ μm^2/s). **b**, *Top panel,* Z-projection of fluorescence intensity (increasing from blue to red) of a BtuB-ColE9^{AF488} complex on a JM83 cell. *Middle panel,* the fluorescence intensity in consecutive images (30 fps) is displayed for a typical fluorescent spot. The intensity and single-step photobleaching behaviour were consistent

with a single membrane complex being tracked. *Bottom panel*, MSD was calculated for individual BtuB-ColE9^{AF488} complexes (*N = 62*) that displayed single-step photobleaching behaviour, could be tracked for at least 1.7 s prior to photobleaching (error is reported as SEM) and were not immobilised on the quartz surface ($MSD_{end\ of\ trajectory} > 0.008$, determined for surface bound ColE9^{AF488} in the same samples). The MSD value rapidly approached an asymptotic value that was consistent with restricted lateral diffusion. Linear regression of the MSD for the first 5 time delays (0.033-0.17 s) yielded the planar diffusion coefficient ($D \sim 0.013\ \mu m^2/s$). See Extended Data Table 1 for all fitted values (from a minimum of 4 experimental replicates). **c**, Comparison of experimental MSD for BtuB-ColE9^{AF488} complexes from panel b (*open circles*) with mean output from Monte Carlo simulations (solid blue line) of two-dimensional diffusion ($D = 0.14\ \mu m^2/s$, association time of 0.2 s ($= k^{-1}$), and 15% volume occupancy) in a curved, crowded membrane typical of a rod-shaped bacterium, which is illuminated by an evanescent field (penetration depth = 150 nm). Here lateral D was identical to the value observed for monomeric BtuB diffusing in PSMs (Extended Data Fig. 5c). The lower apparent lateral D measured experimentally (= $0.013\ \mu m^2/s$) indicates the promiscuous PPIs induce temporal corralling. The dashed (blue) lines are the upper and lower 99.75% confidence limits for the mean (n = 5000 trajectories). See Methods for details of the Monte Carlo simulations. ***d***, MSD plots (± SE) for all confined trajectories (500 in each case) of BtuB-ColE9^{TMR} complexes diffusing in PSMs, red data points in Fig. 4b (panels 3 and 4), main text. [BtuB] x1000 data (*open circles*) is compared to data for native levels of BtuB (*closed circles*) in the presence of native levels of OmpF (equivalent to [BtuB] x1000). Fits to both sets of data yield values for *D* and confinement diameter, $\sim 0.02\ \mu m^2/s$ and 0.4 μm, respectively, that are very similar to those observed *in vivo*.

Europe PMC Funders Author Manuscripts

Europe PMC Funders Author Manuscripts

Europe PMC Funders Author Manuscripts

Europe PMC Funders Author Manuscripts

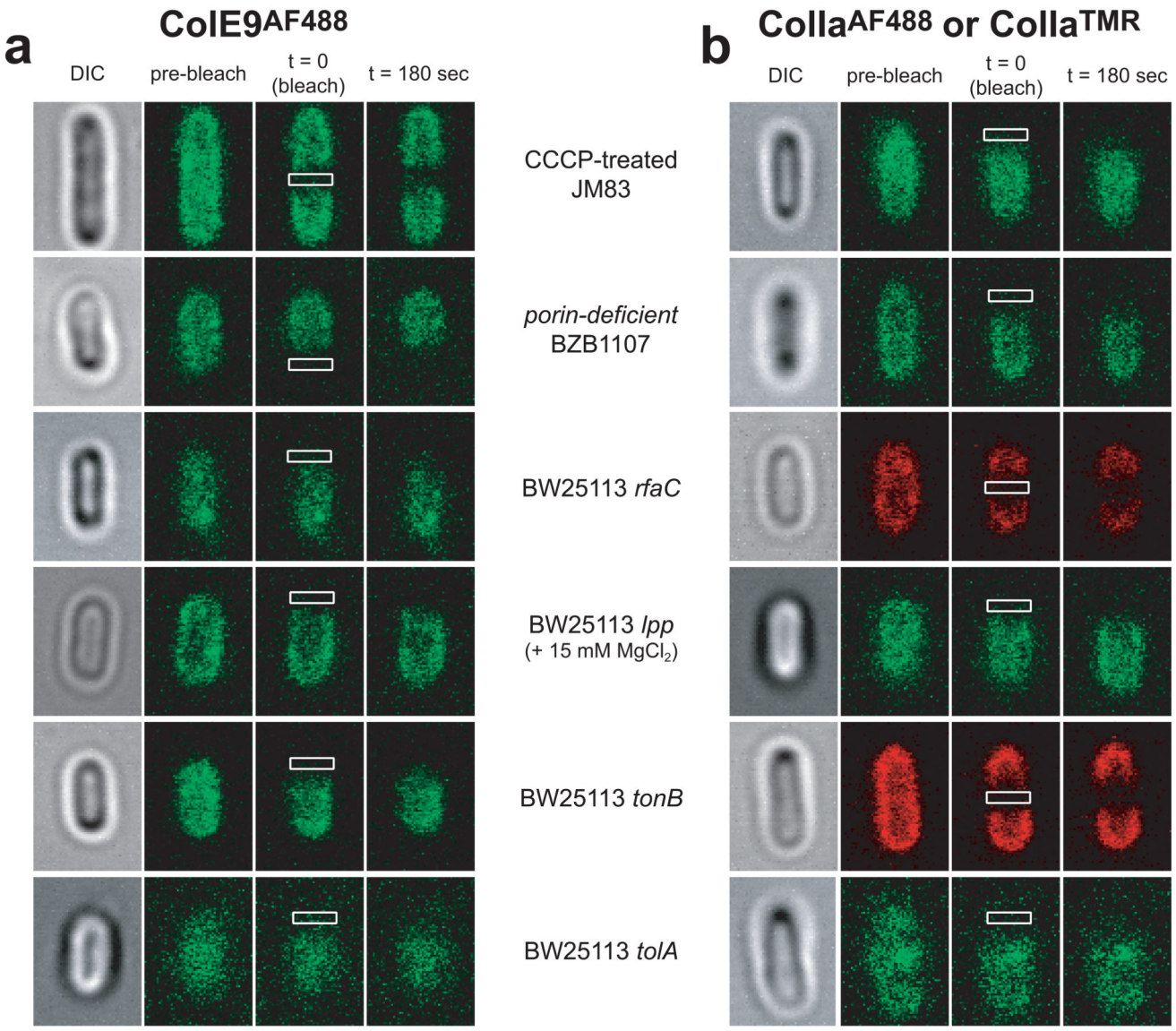

Figure 3. Probing the roles of cell envelope systems in the restricted diffusion of OMPs.

Laser-scanning confocal FRAP microscopy of *E. coli* cells labelled with ColE9^{AF488} for BtuB (***a***) and Colla^{AF488} or Colla^{TMR} for Cir (***b***) was used in conjunction with gene deletions or chemical treatments to probe the involvement of various cell envelope systems in the restricted mobility of OMPs. The rationale for these experiments was two-fold. First, structures or processes within the Gram-negative cell envelope could be responsible for the restricted mobility of OMPs (Extended Data Fig. 1 and 2). Second, FRAP would provide a means of detecting the loss of restricted OMP mobility, resulting in the recovery of fluorescence after photobleaching, if these systems were perturbed. Each panel in the figure shows DIC microscopy images of the bacterial cell followed by pre-bleach, bleach (t = 0) and post-bleach (t = 3 min) fluorescent images of the same cell. All microscopy images are 3.03 μm x 4.17 μm. *Top-to-bottom*; CCCP treatment (0.1 mM) of *E. coli* JM83 cells assessed the impact of dissipating the proton-motive force (pmf) across the IM. *E. coli*

Europe PMC Funders Author Manuscripts

Europe PMC Funders Author Manuscripts

BZB1107 cells (*ompR vlamB ompF*::Tn*5*) are deficient for the major OM porins OmpF and OmpC. *E. coli* BW25113 *rfaC* (JW3596) is a deep-rough mutant in which the outer core of the LPS is truncated. *E. coli* BW25113 *lpp* (JW1667) is a deletion of Braun's lipoprotein, an OM lipoprotein that is one of the most abundant proteins in *E. coli*. ~40% of Lpp is covalently attached to the underlying peptidoglycan. *E. coli* BW25113 *tonB* (JW5195) is deleted for TonB, a protein that spans the periplasm and couples the pmf across the IM with transport of nutrients through OM proteins such as BtuB and Cir. Colla depends on TonB for import into bacteria. *E. coli* BW25113 *tolA* (JW0729) is deleted for TolA, a protein that spans the periplasm and couples pmf with stabilisation of the OM. ColE9 depends on TolA for import into bacteria. Other *E. coli* K-12 deletion strains tested (but not shown) include *pal* (JW0731), an OM lipoprotein, and *ompA* (JW0940), both of which have domains that form non-covalent contacts with the peptidoglycan cell wall. As the data in the figure show, no mutation or condition resulted in the recovery of fluorescence in FRAP experiments from which we infer these systems/processes are not responsible for the restricted mobility of OMPs. Finally, we tested a mutation of ColE9 in which the first 83 amino acids of the colicin were deleted ($^{\Delta 1\text{-}83}$ ColE9) but where the inactivating disulphide across the R-domain remained in place. The N-terminal 83 residues contain protein-protein interaction epitopes for OmpF as well as TolB in the periplasm. No change in FRAP behaviour (not shown) was observed demonstrating that interactions made by the colicin at the cell surface are not responsible for the restricted mobility of the OMP to which it is bound. These experiments were done in duplicate (one representative set of images for each condition is presented in the figure).

Europe PMC Funders Author Manuscripts

Europe PMC Funders Author Manuscripts

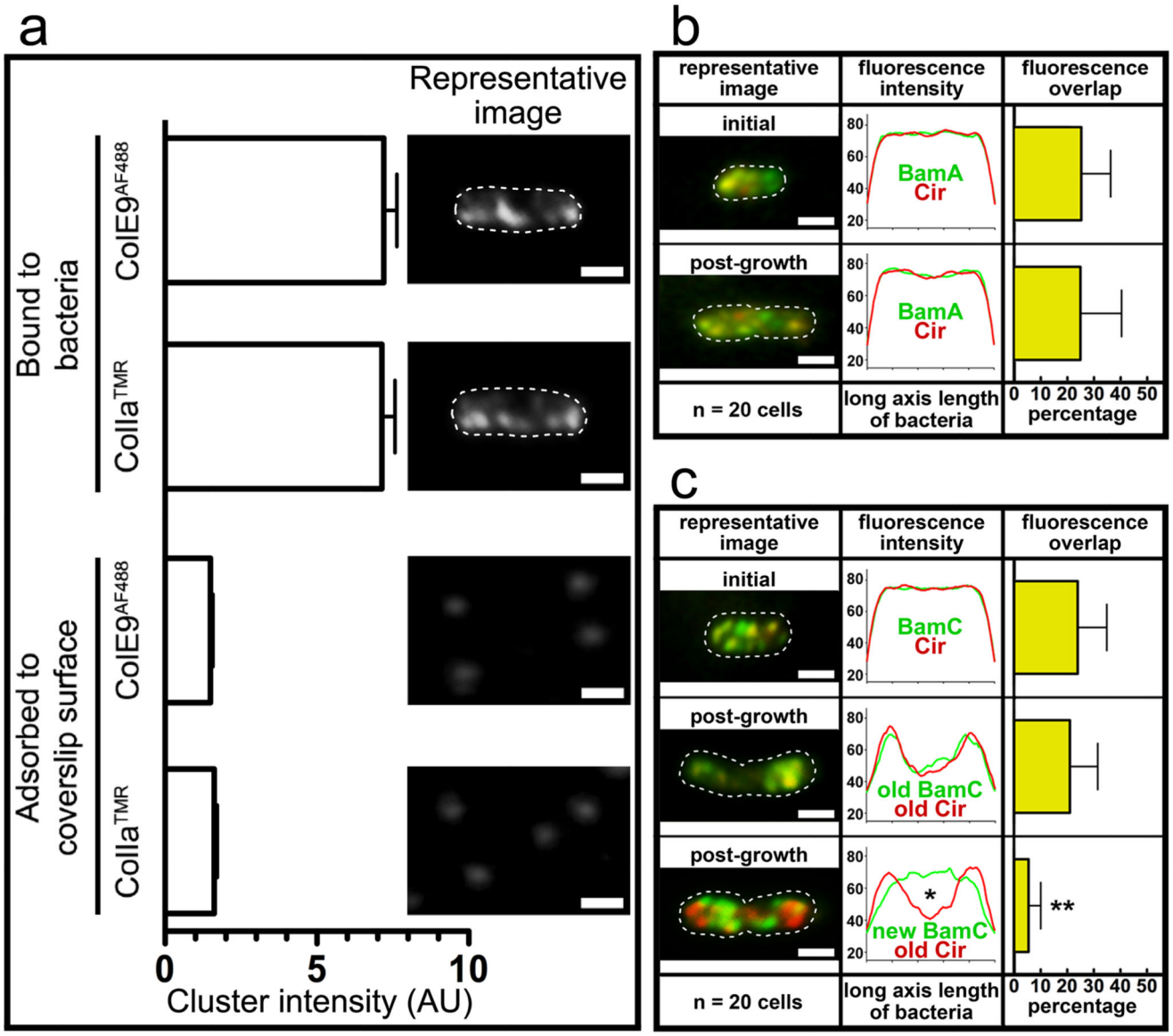

Figure 4. ***a,*** **Estimation of the number of BtuB and Cir proteins within OMP islands.**
The scatter plots show the distribution of relative intensity of ColE9^{AF488} and Colla^{TMR} fluorescence signals when bound to their specific OMPs in bacteria or adhered to surfaces. The right hand panels show representative TIRFM images that were used for the analysis. Fluorescence signals corresponded to a stack of 100 frames (30 fps) and were relatively stable in time and space. Scale bar = 1 μm. The mean value (± SEM) for each distribution is shown by the histograms. We normalised the data for colicins adhered to bacteria using the mean intensity for surface-adhered ColE9^{AF488} and Colla^{TMR} (300 nM), assuming these correspond to one molecule (~1 AU). From this normalisation, OMP islands on average contained ~7 labelled OMPs although values ranged from 1 to 19 labelled OMPs. The entire experiment was conducted twice, the replicate showing the same mean value of OMPs per island. ***b*** **Co-localisation of BamA with Cir.** TIRFM images (sum of 100 frames) of *E. coli* JWD3 cells expressing HA-tagged BamA detected by Alexa^{488}-labelled anti-HA

Europe PMC Funders Author Manuscripts

Europe PMC Funders Author Manuscripts

antibody19. Cir was detected by Colla^{TMR} labelling before and after a 1 h period of growth. BamA shows significant co-localisation (31 (± 7) % for 112 OMP islands visualised across 20 cells, co-localisation error is reported as SDM) with Cir within OMP islands. Due to weak binding of the anti-HA antibody it was not possible to perform more detailed growth experiments as for BamC. ***c*, Co-localisation of BamC with Cir**. TIRFM images (sum of 100 frames) for *E. coli* JM83 cells stained with Alexa^{488} labelled anti-BamC antibody and Colla^{TMR} showing co-localization within OMP islands that move to the poles in cells undergoing division. Temporal separation of BamC and the Cir labels by a 1 h period of growth, where old BamC was first blocked with unlabelled antibody, showed that old Cir was localized primarily at the old poles (*red label*) while new BamC-containing islands appeared in non-polar regions of the cell (*green label*). The average fluorescence distributions and co-localisation histograms (error is reported as SEM) shown in panels b and c are from 20 cells in each case. * indicates a significant difference in fluorescence distribution ($0.01 < p < 0.1$) and ** denotes a very significant difference in co-localisation ($p < 0.001$) as determined using a student T-test and a non-parametric Mann-Whitney test, respectively.

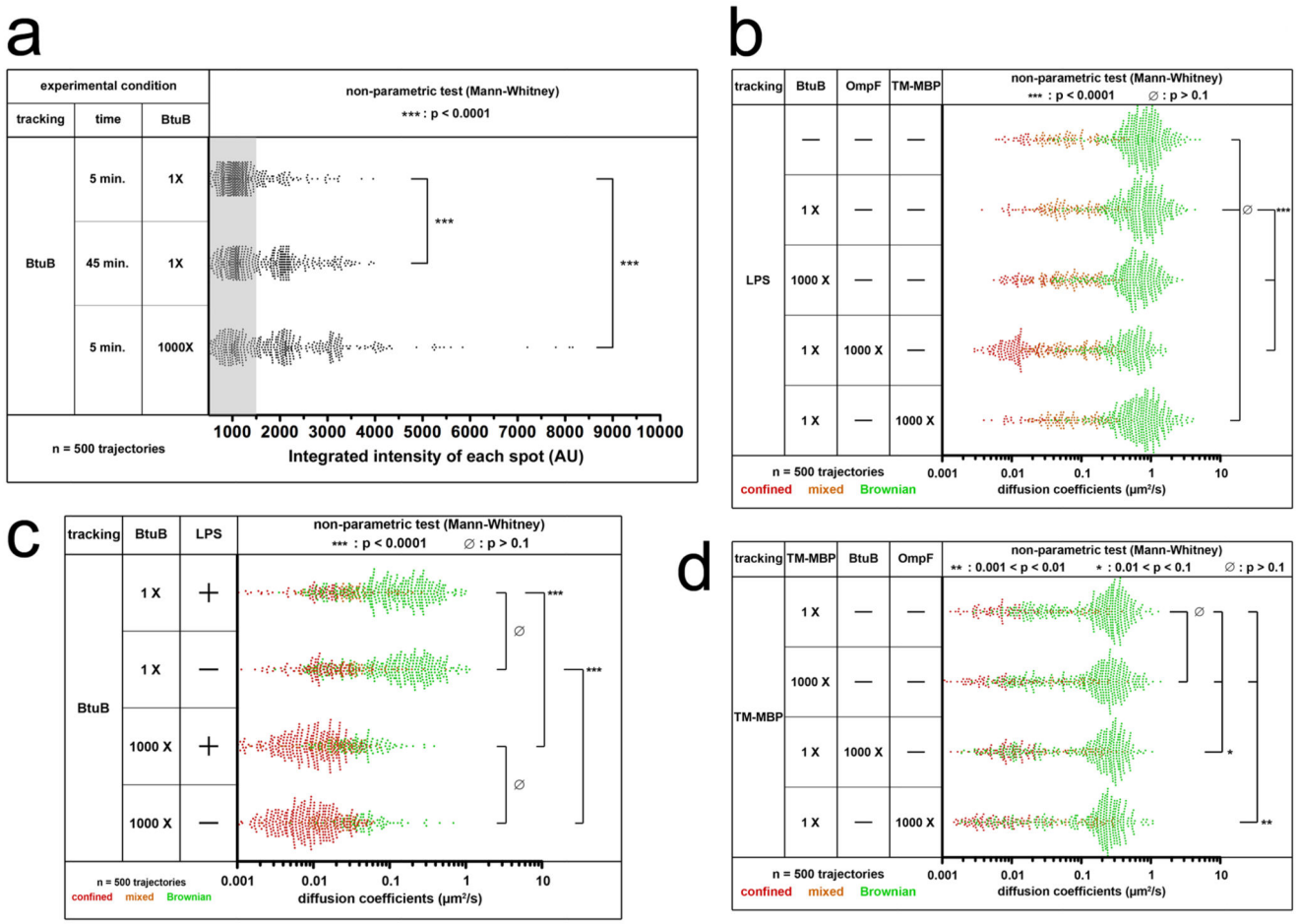

Figure 5. Influence of membrane components on diffusion in polymer-supported membranes.

a, Analysis of the relative fluorescence intensity of BtuB-ColE9^{TMR} suggested significant self-association of BtuB, which was time and concentration dependent. The grey area corresponds to the range of intensities where single step photobleaching was observed and which were the molecules tracked in our experiments. ***b***, Distribution of diffusion coefficient when tracking BtuB-ColE9^{TMR} incorporated into a polymer-supported bilayer that contains a ratio of 17:1 or 0:1 LPS:BtuB. Addition of LPS did not alter significantly the diffusion behaviour of BtuB in these artificial membranes. ***c***, Distribution of diffusion coefficient when tracking LPS$^{BODIPY®}$ incorporated into a polymer-supported bilayer at a ratio of 17:1 ratio LPS:BtuB. High concentrations of BtuB or OmpF, but not of TM-MBP, induced significant trapping of some LPS molecules. ***d***, Distribution of diffusion coefficients when tracking TM-MBP^{Cy5} incorporated into a polymer-supported bilayer. High concentrations of BtuB or OmpF, but not of TM-MBP, induced a slight but significant trapping of some TM-MBP molecules. All experiments were done in duplicate (one set are presented in the figure) and differences in diffusion coefficient determined using a non-parametric Mann-Whitney test.

Europe PMC Funders Author Manuscripts

Europe PMC Funders Author Manuscripts

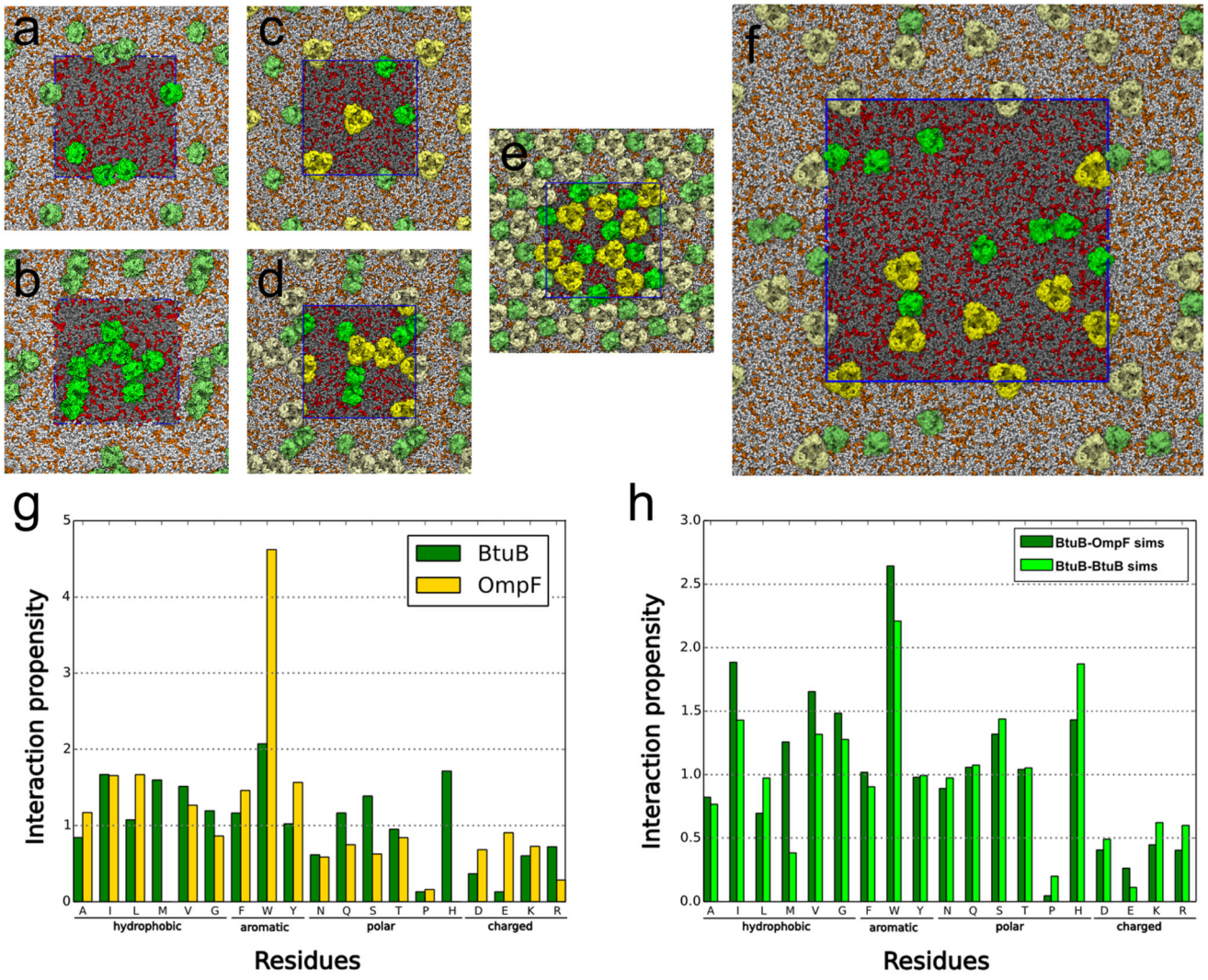

Figure 6. Final snapshots of OmpF (yellow) and BtuB (green) positions for coarse grain MD simulations.

Each patch (~30 x 30 nm^2 for ***a-e***, ~60 x 60 nm^2 for ***f***) contained, ***a***, two BtuB; ***b***, nine BtuB; ***c***, two OmpF trimers and two BtuB monomers; ***d***, four OmpF and five BtuB; ***e***, eight OmpF and eight BtuB; ***f***, eight OmpF and eight BtuB. In each case, the single unit cell is darkened and outlined in blue. Lipids are shown in grey (PE) and red (PG). See Extended Data Fig. 7 and Table 2 for further details. ***g***, Propensity for BtuB (*green*) and OmpF (*yellow*) residues to be at the protein-protein interface based on simulations of BtuB-OmpF mixtures. A propensity greater than one indicates that a residue occurs more frequently at the interaction interface than on the protein surface. ***h***, BtuB residue propensities for residue types at the interface between two BtuB monomers, based on simulations containing OmpF and BtuB (*dark green)*, or just BtuB (*light green)*. The two propensities are similar. Note that the sampling in terms of homo-interactions of BtuBs in the OmpF-BtuB simulation is less than in the simulation containing only BtuB due to the starting positions of the proteins in OmpF-

Europe PMC Funders Author Manuscripts
Europe PMC Funders Author Manuscripts

BtuB simulations, which favour hetero-interactions between BtuB and OmpF. See Methods for details about the calculation of the propensity values.

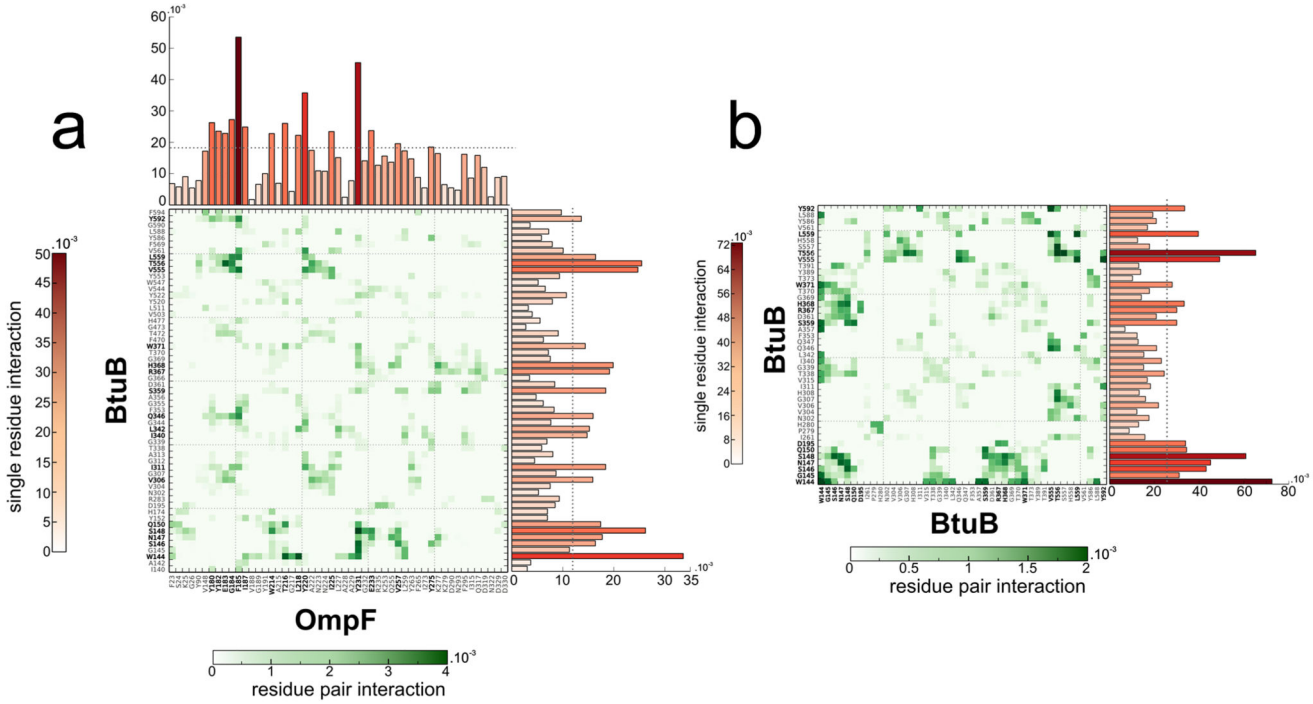

Figure 7. Residues that mediate BtuB-OmpF (*a*) and BtuB-BtuB (*b*) interactions in MD simulations.

The interaction matrix charts the frequency of interaction between any pair of BtuB and OmpF residues, as a proportion of the total number of interactions that occurred, from high proportional frequency (*dark green*) to low (*white*). Depicted here is a subset of the entire interaction matrix, showing only the residues which engaged in interactions with the other protein over a threshold value; any BtuB residue which had a proportional interaction frequency of more than 1 x 10^{-3} with any OmpF residue is shown, and similarly for any OmpF residue. On each side, residues with interaction frequency values above *c.a.* one third of the maximum value of interaction are highlighted in bold. The bar plots show the proportional interaction frequencies of each single BtuB (side) and OmpF (top) residue, for the subset of residues that are shown in the interaction matrix. See Methods for a full mathematical explanation of the interaction value calculations. Bar plots are coloured according to the bar values, from high proportional interaction frequency (*dark red*) to low (*white*). This is consistent with the colour scheme in Figure 4e. Note the matrix in *b* is symmetric.

Europe PMC Funders Author Manuscripts
Europe PMC Funders Author Manuscripts

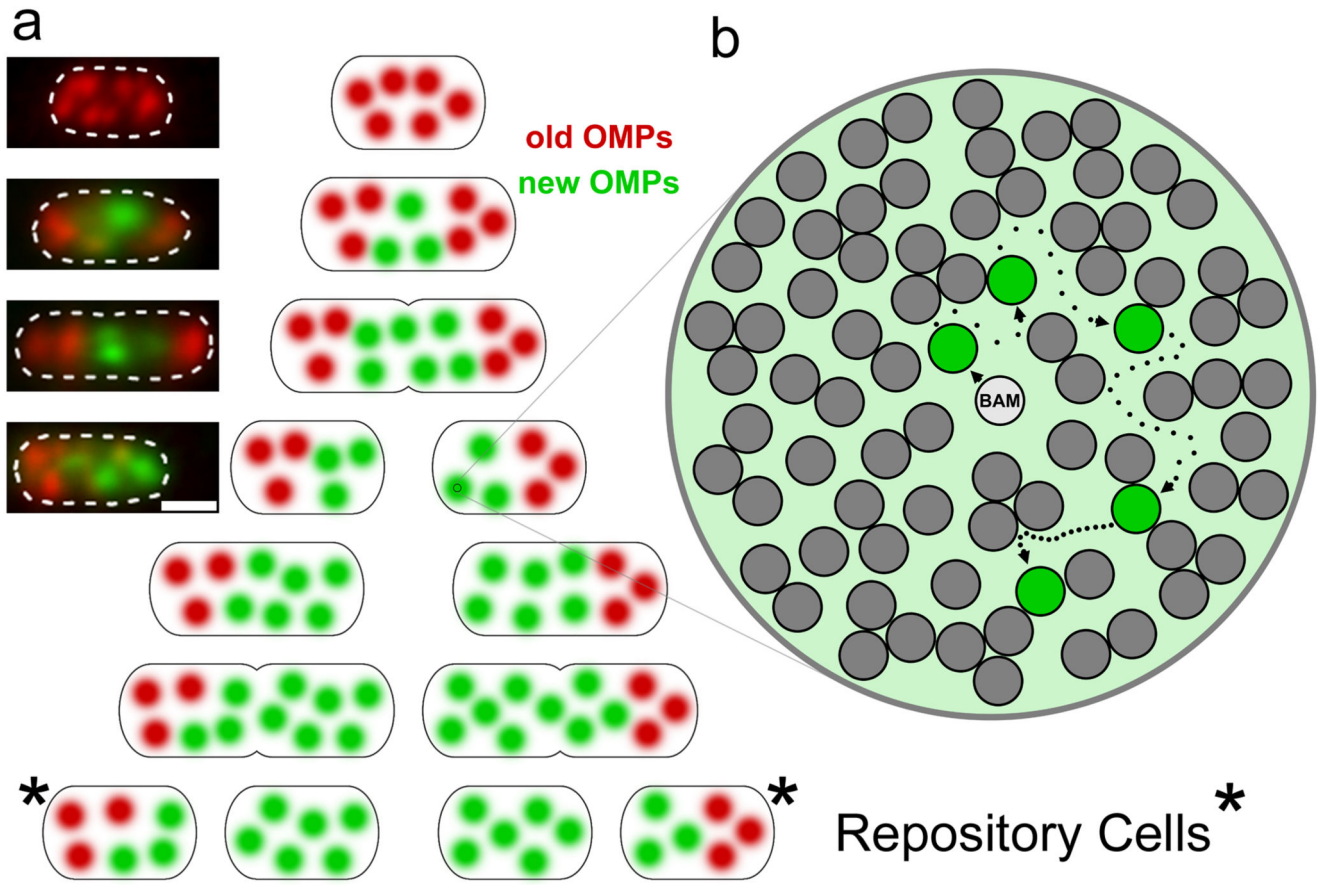

Figure 8. Binary OMP partitioning and its relationship to biogenesis and organisation of OMP islands.

a, Model depicting the appearance of new OMP islands (*green*) within growing cells containing old OMP islands (*red*) in which OMP biogenesis has ceased. The TIRFM images of single cells shown alongside the different stages were taken from cell growth experiments (same experiments as shown in Fig. 2, main text). The model highlights how new OMP islands appear mostly at mid-cell, their creation in conjunction with cell elongation forces old OMP islands towards the poles. The result is binary turnover when the cell divides. The bulk of the old OMPs are retained at the poles of Repository Cells, which are created at every cell division. It remains unclear why OMP biogenesis ceases in old OMP islands. It is also unclear whether the architecture of the poles (e.g. membrane curvature) plays a role in retaining old OMPs or whether this is entirely a consequence of continued growth and biogenesis in daughter cells. Nevertheless, the outcome of such a mechanism is that within just two divisions cells appear that do not have any of the original old OMPs. The stochastic nature of the process occasionally results in some old OMP islands not partitioning with the old pole (e.g. main text Fig. 2b, panel 3 TIRFM image), which likely explains why the process is not a pure binary mechanism (if it were, values of 100% would be expected in the histogram shown in Fig. 1f, main text). We speculate that the lack of intermixing between OMP islands, which is consistent with the absence of fluorescence recovery in *in vivo* FRAP experiments (Extended Data Fig. 1), may be due to the very high density of OMPs

Europe PMC Funders Author Manuscripts
Europe PMC Funders Author Manuscripts

Europe PMC Funders Author Manuscripts

Europe PMC Funders Author Manuscripts

(particularly porins)25 within islands separated by densely packed LPS. ***b***, Model depicting the organisation of an individual OMP island and the movement of an OMP within it. OMP islands contain one or more Bam complexes (see main text Fig. 3). Here, we show a single Bam machine having just deposited an OMP (*green circle*) in the OM. The new OMP diffuses laterally in the membrane but becomes increasingly restricted due to promiscuous interactions with other OMPs (*grey circles*), which is consistent the confinement experienced by OMPs *in vitro* and *in vivo* (main text Fig. 4b and Extended Data Fig. 2) and with MC and MD simulations (main text Fig. 4 c, d and Extended Data Fig. 2c, 6 and 7). Only a fraction of the OMPs presumed to be present within an OMP island are shown.

Extended Data Table 1

Comparison of BtuB and Cir diffusion parameters from the present work with those reported for other Gram-negative OMPs and IMPs in the literature.

OMP and IMP data are shown above and below the grey bar, respectively. Diffusion coefficients (*D*) were obtained from linear regression of the first 4-5 time steps. See Methods and Extended Data Fig. 2 for details. Two strains were used for the single molecule studies reported in the present paper, the standard lab strain *E. coli* JM83 and a strain in which the major porins OmpF and OmpC had been deleted, *E. coli* BZB110758. BtuB labelling was achieved using either full-length, fluorescently-labelled ColE9 or a variant lacking the first 52 amino acids, a disordered region of the toxin that contains an OmpF binding site and a binding epitope for the periplasmic protein TolB10. Cir labelling was achieved using fluorescently-labelled Colla. The single-molecule trajectories analysed for each condition represent a minimum of 4 experimental replicates.

Protein	D(μm^2/s)	Confinement diameter(μm)	Reference
LamB	0.15	0.03	55
BtuB	0.05,0.10	NR	56
OmpF	0.006	0.1	56
BtuB (ColE9, JM83 cells)	0.013 (N=62)	0.6	Present work
BtuB ($\Delta^{1\text{-}52}$ ColE9, JM83 cells)	0.0081 (N=51)	0.5	Present work
BtuB (ColE9, BZB1107 cells)	0.018 (N=30)	0.5	Present work
Cir (Colla, JM83 cells)	0.019 (N=41)	0.6	Present work
Cir (Colla, BZB1107 cells)	0.011 (N=14)	0.5	Present work
Plec-YFP	0.012		39
MotB-GFP	0.009		40
TatA-YFP	0.1-0.01		57

NR, not reported

Europe PMC Funders Author Manuscripts

Europe PMC Funders Author Manuscripts

Extended Data Table 2

Summary of coarse grain MD simulations for BtuB or OmpF systems and OmpF/BtuB mixtures at differing levels of crowding.

See Methods and Extended Data Fig. 6 and 7 for details. Increasing the density of proteins decreased their calculated diffusion coefficients, although the magnitude of the change was contingent on the size of the system, in agreement with recent modelling studies on crowded membranes24,49 and with the PSM data shown in Fig. 4b. While diffusion coefficients are qualitatively in agreement with our experimental results the time scale remains too short to enable quantitative comparisons, as has been discussed in a number of other CG MD studies54.

Number of proteins		Dimensions (nm^2)	Protein fractional ratio (%)	Simulation time (μs)	Diffusion coefficient ($\mu m^2 s$)	
BtuB	OmpF				BtuB	OmpF
1	0	30 × 30	2	10	11.53 ± 0.33	---
4	0	30 × 30	9	10	8.16 ± 0.78	---
9	0	30 × 30	19	10	2.88 ± 0.94	---
36	0	60 × 60	19	10	6.71 ± 1.00	---
0	1	30 × 30	4	10	---	6.64 ± 1.72
2	2	30 × 30	13	10	9.46 ± 0.78	5.17 ± 1.55
8	8	60 × 60	13	10	13.94 ± 2.64	11.58 ± 1.29
5	4	30 × 30	28	10	2.35 ± 0.06	1,89 ± 0,18
18	18	60 × 60	29	10	2.25 ± 1.74	2.22 ± 1.38
8	8	30 × 30	52	10	0.27 ± 0.00	0.26 ± 0.03

Supplementary Material

Refer to Web version on PubMed Central for supplementary material.

Acknowledgements

We thank the Micron facility (University of Oxford) and the York Technology Facility (University of York) for access to microscopy facilities. The authors also thank Susan Buchanan (NIH) and Karen Jakes (Albert Einstein) for anti-BamC antibody and Colla plasmids, Ian Henderson (Birmingham) for HA-tagged BamA constructs, Colin Robinson (University of Kent) for TatA-GFP construct, Karin Heurlier (York) and James Pullen (Fujifilm, Middlesborough) for PCR screening of deletion strains, Amit Sharma (University of Leeds) for the design of the inactivating disulphide bond in Colla and Pierre Emmanuel Milhiet (Montpellier) and his group for providing optimised PATRACK single-molecule tracking software. A.L.D. and M.C. thank T. Reddy for fruitful discussions and assistance with diffusion calculations. U.S. and C.G.B. thank the Biology Electronic and Mechanical Workshops (University of York) for custom fabrications, and Gregory Mashanov (National Institute for Medical Research, London) for custom image acquisition software. We also thank Ben Berks (University of Oxford) for helpful comments on the manuscript. C.G.B. acknowledges the Royal Society (2004/R1) and the University of York (Research Priming Fund) for financial support used to develop the TIRFM. PR acknowledges the late Rachid Saadia for his unwavering support. M.S.P.S. acknowledges access to the UK supercomputer ARCHER for MD simulations. This work was supported by grants to C.K. and C.G.B. (BBSRC LoLa grant BB/G020671/1), J.P.

(Deutsche Forschungsgemeinschaft SFB 944) and M.S.P.S. (BBSRC BB/L002558/1, Wellcome Trust WT092970MA).

References

1. van Elsas JD, Semenov AV, Costa R, Trevors JT. Survival of *Escherichia coli* in the environment: fundamental and public health aspects. ISME J. 2011; 5:173–183. [PubMed: 20574458]
2. Tenaillon O, Skurnik D, Picard B, Denamur E. The population genetics of commensal *Escherichia coli*. Nat Rev Microbiol. 2010; 8:207–217. [PubMed: 20157339]
3. Morabito, S., editor. Pathogenic Escherichia coli: Molecular & cellular microbiology. Caister Academic Press; 2014.
4. Vogel J, Papenfort K. Small non-coding RNAs and the bacterial outer membrane. Curr Op Microbiol. 2006; 9:605–611.
5. Nikaido H. Molecular basis of bacterial outer membrane permeability revisited. Microbiol Mol Biol Rev. 2003; 67:593–656. [PubMed: 14665678]
6. Moon CP, Zaccai NR, Fleming PJ, Gessmann D, Fleming KG. Membrane protein thermodynamic stability may serve as the energy sink for sorting in the periplasm. Proc Natl Acad Sci USA. 2013; 110:4285–4290. [PubMed: 23440211]
7. Hagan CL, Silhavy TJ, Kahne D. β-Barrel membrane protein assembly by the Bam complex. Annu Rev Biochem. 2011; 80:189–210. [PubMed: 21370981]
8. Noinaj N, et al. Structural insight into the biogenesis of beta-barrel membrane proteins. Nature. 2013; 501:385–390. [PubMed: 23995689]
9. Kleanthous C. Swimming against the tide: progress and challenges in our understanding of colicin translocation. Nat Rev Microbiol. 2010; 8:843–848. [PubMed: 21060316]
10. Housden NG, et al. Intrinsically disordered protein threads through the bacterial outer membrane porin OmpF. Science. 2013; 340:1570–1574. [PubMed: 23812713]
11. Shapiro L, McAdams HH, Losick R. Why and how bacteria localize proteins. Science. 2009; 326:1225–1228. [PubMed: 19965466]
12. Housden NG, Loftus SR, Moore GR, James R, Kleanthous C. Cell entry mechanism of enzymatic bacterial colicins: porin recruitment and the thermodynamics of receptor binding. Proc Natl Acad Sci USA. 2005; 102:13849–13854. [PubMed: 16166265]
13. Kurisu G, et al. The structure of BtuB with bound colicin E3 R-domain implies a translocon. Nat Struct Biol. 2003; 10:948–954. [PubMed: 14528295]
14. Buchanan SK, et al. Structure of colicin I receptor bound to the R-domain of colicin la: implications for protein import. EMBO J. 2007; 26:2594–2604. [PubMed: 17464289]
15. Mullineaux CW, Nenninger A, Ray N, Robinson C. Diffusion of green fluorescent protein in three cell environments in *Escherichia coli*. J Bacteriol. 2006; 188:3442–3448. [PubMed: 16672597]
16. Verhoeven GS, Dogterom M, den Blaauwen T. Absence of long-range diffusion of OmpA in *E. coli* is not caused by its peptidoglycan binding domain. BMC Microbiol. 2013; 13:66. [PubMed: 23522061]
17. Smit J, Nikaido H. Outer membrane of Gram-negative bacteria. XVIII. Electron microscopic studies on porin insertion sites and growth of cell surface of *Salmonella typhimurium* . J Bacteriol. 1978; 135:687–702. [PubMed: 355240]
18. Ursell TS, Trepagnier EH, Huang KC, Theriot JA. Analysis of surface protein expression reveals the growth pattern of the Gram-negative outer membrane. PLoS Comput Biol. 2012; 8:e1002680. [PubMed: 23028278]
19. Browning DF, et al. Mutational and Topological Analysis of the *Escherichia coli* BamA Protein. PLoS One. 2013; 8:e84512. [PubMed: 24376817]
20. Webb CT, et al. Dynamic association of BAM complex modules includes surface exposure of the lipoprotein BamC. J Mol Biol. 2012; 422:545–555. [PubMed: 22683355]
21. Roder F, et al. Reconstitution of membrane proteins into polymer-supported membranes for probing diffusion and interactions by single molecule techniques. Anal Chem. 2011; 83:6792–6799. [PubMed: 21838222]

Europe PMC Funders Author Manuscripts

Europe PMC Funders Author Manuscripts

Europe PMC Funders Author Manuscripts

22. White JC, DiGirolamo PM, Fu ML, Preston YA, Bradbeer C. Transport of vitamin B_{12} in *Escherichia coli*. Location and properties of the initial B_{12}-binding site. J Biol Chem. 1973; 248:3978–3986. [PubMed: 4196588]
23. Casuso I, et al. Characterization of the motion of membrane proteins using high-speed atomic force microscopy. Nat Nanotech. 2012; 7:525–529.
24. Goose JE, Sansom MS. Reduced lateral mobility of lipids and proteins in crowded membranes. PLoS Comput Biol. 2013; 9:e1003033. [PubMed: 23592975]
25. Jaroslawski S, Duquesne K, Sturgis JN, Scheuring S. High-resolution architecture of the outer membrane of the Gram-negative bacteria *Roseobacter denitrificans*. Mol Microbiol. 2009; 74:1211–1222. [PubMed: 19843216]
26. Stewart EJ, Madden R, Paul G, Taddei F. Aging and death in an organism that reproduces by morphologically symmetric division. PLoS Biol. 2005; 3:e45. [PubMed: 15685293]
27. Laloux G, Jacobs-Wagner C. How do bacteria localize proteins to the cell pole? J Cell Sci. 2014; 127:11–19. [PubMed: 24345373]
28. Qiao S, Luo Q, Zhao Y, Zhang XC, Huang Y. Structural basis for lipopolysaccharide insertion in the bacterial outer membrane. Nature. 2014; 511:108–111. [PubMed: 24990751]
29. Ieva R, Tian P, Peterson JH, Bernstein HD. Sequential and spatially restricted interactions of assembly factors with an autotransporter beta domain. Proc Natl Acad Sci USA. 2011; 108:E383–391. [PubMed: 21646511]
30. Konovalova A, Perlman DH, Cowles CE, Silhavy TJ. Transmembrane domain of surface-exposed outer membrane lipoprotein RcsF is threaded through the lumen of beta-barrel proteins. Proc Natl Acad Sci USA. 2014; 111:E4350–4358. [PubMed: 25267629]
31. Baba T, et al. Construction of *Escherichia coli* K-12 in-frame, single-gene knockout mutants: the Keio collection. Mol Syst Biol. 2006; 2:2006 0008.
32. Penfold CN, et al. Flexibility in the receptor-binding domain of the enzymatic colicin E9 is required for toxicity against *Escherichia coli* cells. J Bacteriol. 2004; 186:4520–4527. [PubMed: 15231784]
33. Garinot-Schneider C, Pommer AJ, Moore GR, Kleanthous C, James R. Identification of putative active-site residues in the DNase domain of colicin E9 by random mutagenesis. J Mol Biol. 1996; 260:731. [PubMed: 8709151]
34. Roder F, Birkholz O, Beutel O, Paterok D, Piehler J. Spatial organization of lipid phases in micropatterned polymer-supported membranes. J Am Chem Soc. 2013; 135:1189–1192. [PubMed: 23289715]
35. Yin J, et al. Genetically encoded short peptide tag for versatile protein labeling by Sfp phosphopantetheinyl transferase. Proc Natl Acad Sci USA. 2005; 102:15815–15820. [PubMed: 16236721]
36. Ray N, Nenninger A, Mullineaux CW, Robinson C. Location and mobility of twin arginine translocase subunits in the *Escherichia coli* plasma membrane. J Biol Chem. 2005; 280:17961–17968. [PubMed: 15728576]
37. Mashanov GI, Molloy JE. Automatic detection of single fluorophores in live cells. Biophys J. 2007; 92:2199–2211. [PubMed: 17208981]
38. Kusumi A, Sako Y, Yamamoto M. Confined lateral diffusion of membrane receptors as studied by single particle tracking (nanovid microscopy). Effects of calcium-induced differentiation in cultured epithelial cells. Biophys J. 1993; 65:2021–2040. [PubMed: 8298032]
39. Deich J, Judd EM, McAdams HH, Moerner WE. Visualization of the movement of single histidine kinase molecules in live Caulobacter cells. Proc Natl Acad Sci USA. 2004; 101:15921–15926. [PubMed: 15522969]
40. Leake MC, et al. Stoichiometry and turnover in single, functioning membrane protein complexes. Nature. 2006; 443:355–358. [PubMed: 16971952]
41. Schneider CA, Rasband WS, Eliceiri KW. NIH Image to ImageJ: 25 years of image analysis. Nat Methods. 2012; 9:671–675. [PubMed: 22930834]
42. Zinchuk V, Wu Y, Grossenbacher-Zinchuk O, Stefani E. Quantifying spatial correlations of fluorescent markers using enhanced background reduction with protein proximity index and correlation coefficient estimations. Nat Protoc. 2011; 6:1554–1567. [PubMed: 21959238]

Europe PMC Funders Author Manuscripts

43. Degrip WJ, Vanoostrum J, Bovee-Geurts PH. Selective detergent-extraction from mixed detergent/lipid/protein micelles, using cyclodextrin inclusion compounds: a novel generic approach for the preparation of proteoliposomes. Biochem J. 1998; 330:667–674. [PubMed: 9480873]
44. Vogelsang J, et al. A reducing and oxidizing system minimizes photobleaching and blinking of fluorescent dyes. Angewandte Chemie. 2008; 47:5465–5469. [PubMed: 18601270]
45. Espenel C, et al. Single-molecule analysis of CD9 dynamics and partitioning reveals multiple modes of interaction in the tetraspanin web. J Cell Biol. 2008; 182:765–776. [PubMed: 18710926]
46. Krementsov DN, et al. HIV-1 assembly differentially alters dynamics and partitioning of tetraspanins and raft components. Traffic. 2010; 11:1401–1414. [PubMed: 20727121]
47. Marrink SJ, Risselada HJ, Yefimov S, Tieleman DP, de Vries AH. The MARTINI force field: coarse grained model for biomolecular simulations. J Phys Chem B. 2007; 111:7812–7824. [PubMed: 17569554]
48. Bond PJ, Wee CL, Sansom MS. Coarse-grained molecular dynamics simulations of the energetics of helix insertion into a lipid bilayer. Biochemistry. 2008; 47:11321–11331. [PubMed: 18831536]
49. Bond PJ, Sansom MS. Insertion and assembly of membrane proteins via simulation. J Am Chem Soc. 2006; 128:2697–2704. [PubMed: 16492056]
50. Klauda JB, Brooks BR, Pastor RW. Dynamical motions of lipids and a finite size effect in simulations of bilayers. J Chem Phys. 2006; 125:144710. [PubMed: 17042634]
51. Michaud-Agrawal N, Denning EJ, Woolf TB, Beckstein O. MDAnalysis: A toolkit for the analysis of molecular dynamics simulations. J Comput Chem. 2011
52. Humphrey W, Dalke A, Schulten K. VMD: visual molecular dynamics. J Mol Graph. 1996; 14:33–38. 27–38. [PubMed: 8744570]
53. Jones S, Thornton JM. Principles of protein-protein interactions. Proc Natl Acad Sci USA. 1996; 93:13–20. [PubMed: 8552589]
54. Javanainen M, et al. Anomalous and normal diffusion of proteins and lipids in crowded lipid membranes. Faraday Disc. 2013; 161:397–417. 419–359.
55. Oddershede L, Dreyer JK, Grego S, Brown S, Berg-Sorensen K. The motion of a single molecule, the lambda-receptor, in the bacterial outer membrane. Biophys J. 2002; 83:3152–3161. [PubMed: 12496085]
56. Spector J, et al. Mobility of BtuB and OmpF in the *Escherichia coli* outer membrane: implications for dynamic formation of a translocon complex. Biophys J. 2010; 99:3880–3886. [PubMed: 21156129]
57. Leake MC, et al. Variable stoichiometry of the TatA component of the twin-arginine protein transport system observed by *in vivo* single-molecule imaging. Proc Natl Acad Sci USA. 2008; 105:15376–15381. [PubMed: 18832162]
58. Jeanteur D, et al. Structural and functional alterations of a colicin-resistant mutant of OmpF porin from *Escherichia coli*. Proc Natl Acad Sci USA. 1994; 91:10675–10679. [PubMed: 7524100]

Europe PMC Funders Author Manuscripts

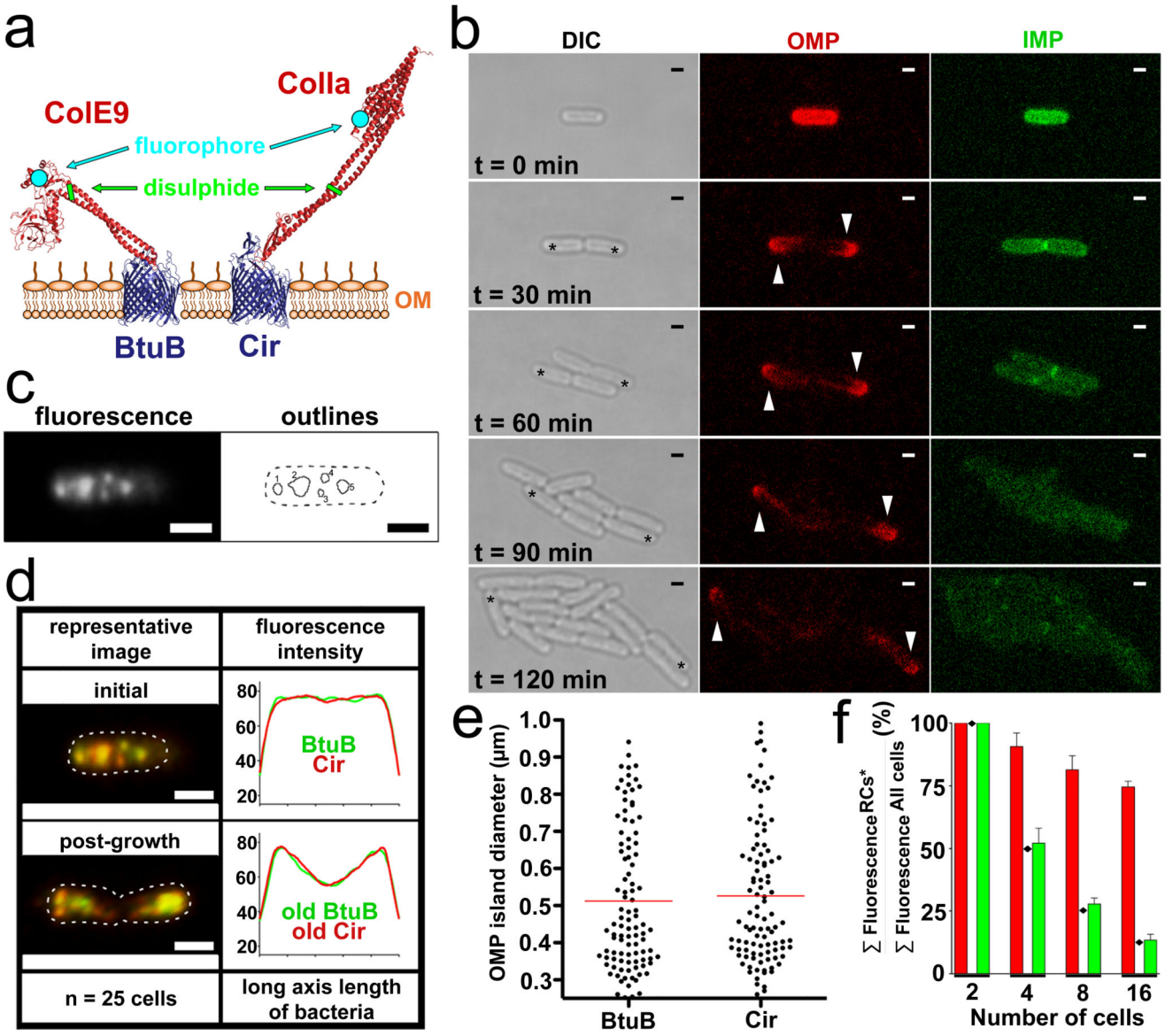

Figure 1. Binary partitioning of OMPS in the *E. coli* OM.

a, Structures of colicins bound to their OMP receptors (1UJW, 1CJH, 1FSJ for ColE9-BtuB model and 2HDI, 1CII for Colla-Cir) highlighting positions of inactivating disulphide bonds and fluorophore labels. ***b***, Distribution of fluorescently-labelled OMP (BtuB-$\Delta^{1\text{-}83}$ ColE9^{TMR}) and IMP (TatA-GFP) in *E. coli* JM83 cells following transient induction with arabinose and imaging by CFM (See Methods). In contrast to TatA-GFP, which distributed in a purely analogue fashion (Fig. 1f), BtuB-$\Delta^{1\text{-}83}$ ColE9^{TMR} segregation was binary. After four divisions two OMP repository cells (RCs; white arrow or asterisk labels) retained the majority of the original OMP. ***c***, *Left-hand panel*, TIRFM image (sum of 100 frames) of BtuB- and Cir-containing OMP islands in *E. coli* JM83 cells labelled with ColE9^{AF488} and Colla^{TMR}, respectively. *Right-hand panel*, automated ImageJ delineation of OMP islands. Inset bar in all panels = 1 μm. ***d***, *Top panel,* False colour image of endogenous, colicin-

Europe PMC Funders Author Manuscripts
Europe PMC Funders Author Manuscripts

labelled BtuB (*green*) and Cir (*red*) showing co-localisation in OMP islands (same cell as in *c*). *Bottom panel*, as above but where cells were grown for 1 h prior to imaging of cells undergoing division. Of the 130 OMP islands analysed before and after growth ($N = 20$ cells/experiment and in duplicate), 40 (± 9) % and 39 (± 7) %, respectively, contained both BtuB and Cir (co-localisation error reported as SDM). ***e***, Size distribution of BtuB- and Cir-containing OMP islands from *c* and *d* above. *Red line* denotes the mean. ***f***, Distribution of fluorescence, shown as a ratio of the two RCs relative to total fluorescence, at each cell division for TatA-GFP (*green bars*) and BtuB-$\Delta^{1\text{-}83}$ ColE9^{TMR} (*red bars*) from five CFM datasets (error reported as SEM). Diamond symbols denote expected ratios for an analogue mechanism.

Europe PMC Funders Author Manuscripts

Europe PMC Funders Author Manuscripts

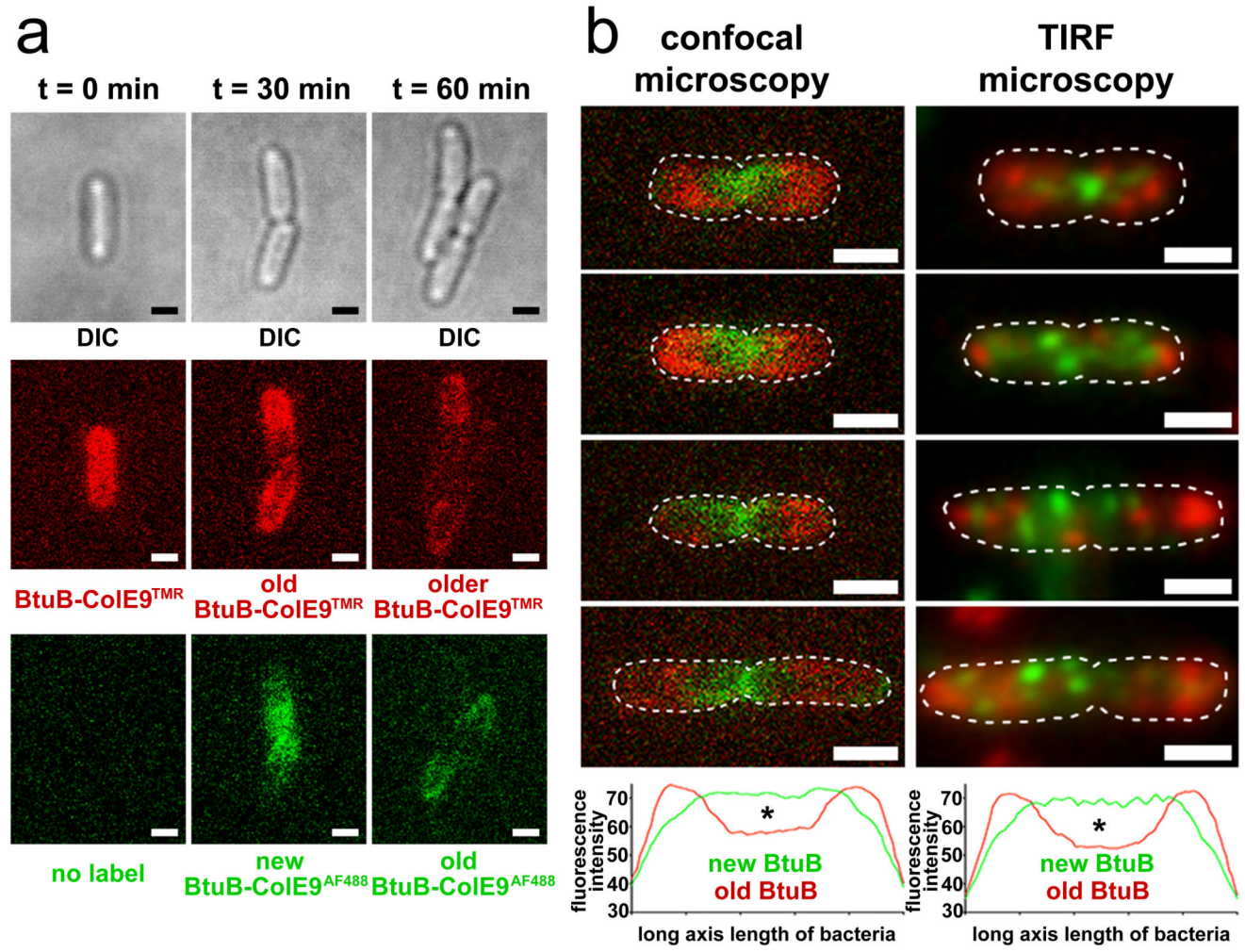

Figure 2. Biogenesis of new OMP islands in the central regions of dividing *E. coli* cells forces old OMP islands towards the poles.

a, Sequential insertion of OMPs in the OM followed by two colour CFM. Growing *E. coli* JM83 cells were labelled initially with ColE9^{TMR} (*red*) (t = 0 min) and then with ColE9^{AF488} (*green*) (t = 30 min) followed by a final growth phase (t = 60 min). Representative data shown from duplicate experiments. ***b*** and ***c***, Confocal and TIRF microscopy images, respectively, of individual dividing *E. coli* JM83 cells from the 30 min time point (panel a). The mean fluorescence distributions shown below the panels are for 20 cells. Single asterisk indicates a significant difference (Mann-Whitney test) in fluorescence distribution ($0.01 < p < 0.1$). Scale bars are 1 μm in all panels. Of the 165 OMP islands analysed by TIRFM at the 30 min time point ($N = 20$ cells/experiment and in duplicate) only 6.4 (± 6.2) % showed overlap of old/new BtuB fluorescence (co-localisation error reported as SDM), emphasising that old OMP islands do not contribute to new OMP synthesis.

Europe PMC Funders Author Manuscripts
Europe PMC Funders Author Manuscripts

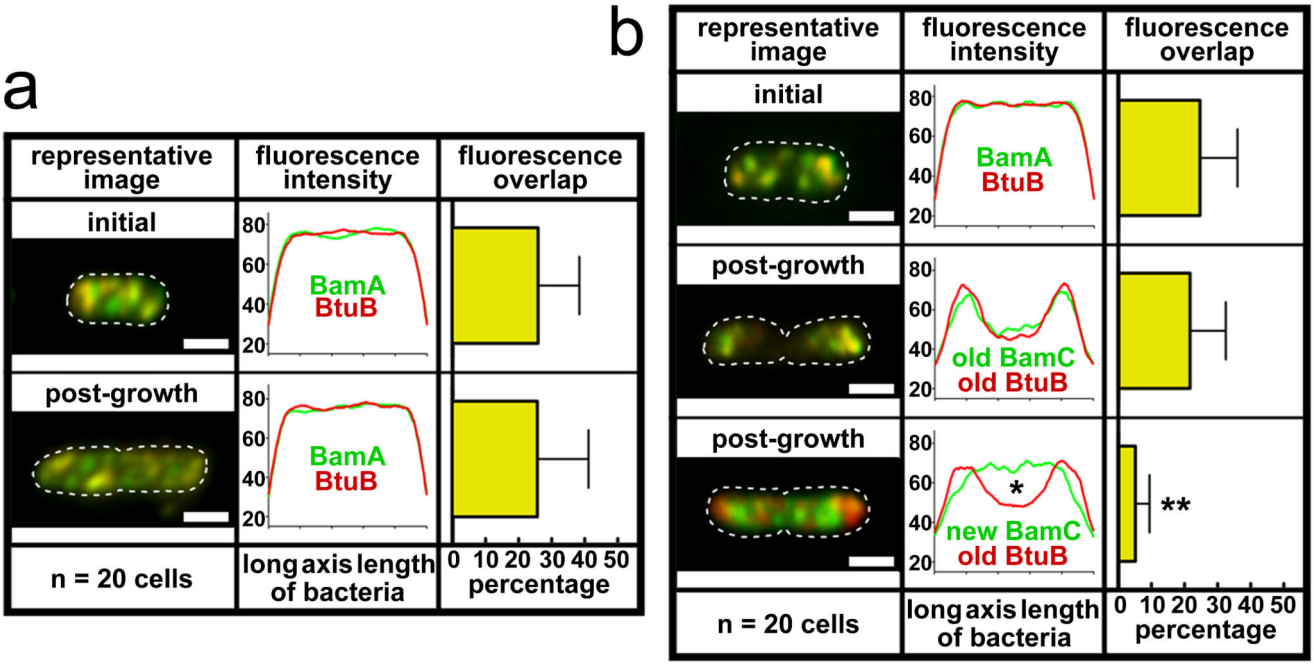

Figure 3. The Bam biogenesis machinery is located within OMP islands that emerge primarily in non-polar regions of the cell and migrate to the poles.

a, TIRFM images (sum of 100 frames) of *E. coli* JWD3 cells producing HA-tagged BamA detected by Alexa^{488}-labelled anti-HA antibody19 (see Methods). ColE9^{TMR} was used to detect endogenous BtuB before and after a 1 h period of growth. Of the 115 OMP islands analysed (co-localisation error reported as SDM), 33 (± 9) % contained both BamA and BtuB. ***b,*** TIRFM images (sum of 100 frames) for *E. coli* JM83 cells stained with Alexa^{488} labelled anti-BamC antibody and ColE9^{TMR} (BtuB). Temporal separation of labels by a 1 h period of growth showed old BtuB-containing islands localized primarily at the poles (*red label*) while new BamC-containing islands localized in non-polar regions (*green label*). The mean fluorescence distributions and co-localisation histograms (error reported as SEM) shown in the panels are from 20 cells in each case. * indicates a significant difference (student T-test) in fluorescence distribution ($0.01 < p < 0.1$) and ** denotes a very significant difference (Mann-Whitney) in co-localisation ($p < 0.001$).

Europe PMC Funders Author Manuscripts
Europe PMC Funders Author Manuscripts

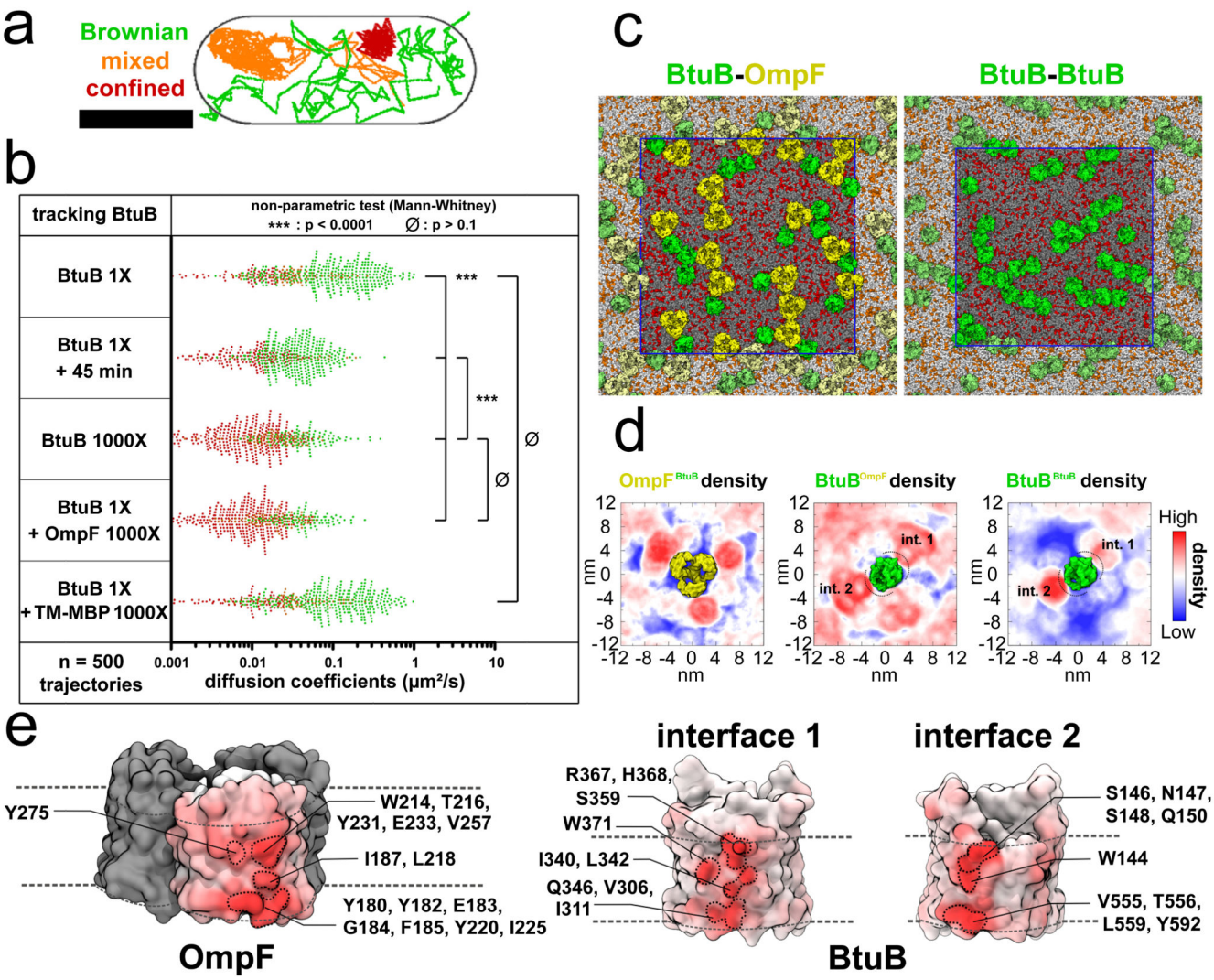

Figure 4. OMPs engage in promiscuous protein-protein interactions.

a, Representative single molecule trajectories (from duplicate experiments) of ColE9^{TMR}-labelled BtuB reconstituted into a PSM overlaid onto a scaled outline of an *E. coli* cell (see Video 6). Molecules exhibited Brownian diffusion, typically extending beyond the boundaries of an *E. coli* cell (*green trace*), mixed (*orange trace*) or confined diffusion (*red trace*). Bar = 1 μm. See Methods. **b**, Initially (at 5 min post deposition of the PSM), and at concentrations found in the OM of *E. coli* (denoted by 1x), BtuB molecules displayed predominantly Brownian diffusion (*panel 1*), but with faster diffusion coefficients than observed *in vivo*. Over time, however, BtuB exhibited slower diffusion suggesting self-association (*panel 2*), an interpretation that was confirmed by raising the BtuB concentration significantly (*panel 3*) which resulted in most of the molecules exhibiting restricted diffusion. The same effect could be elicited using an unrelated OMP, OmpF (*panel 4*), but not maltose binding protein (TM-MBP) tethered to the membrane through a single transmembrane helix (*panel 5*). **c**, Snapshots of a crowded bilayer (~30% and ~20% protein fractional area, for BtuB-OmpF and BtuB-BtuB simulations, respectively) from MD

Europe PMC Funders Author Manuscripts
Europe PMC Funders Author Manuscripts

simulations after 10 μs (see also Extended Data Fig. 6 and 7 and Table 2). OmpF is shown in yellow, BtuB in green. The blue inner square represents the simulation box (60 x 60 nm^2) while the outer region represents the periodic replicates. Lipids in the unit cell were present in a ratio of 3:1 PE (*grey*) and PG (*red*). ***d***, Density plots of the frequency of occurrence of BtuB around OmpF (*left*) and of OmpF around BtuB (*middle*) observed in the BtuB-OmpF simulations, and of BtuB around BtuB (*right*) in the BtuB-BtuB simulations (see Extended Data Fig. 7). ***e,*** High frequency interaction sites at the interface between BtuB and OmpF. Dashed lines represent the position of the bilayer. The OmpF-BtuB interactions were predominantly mediated by hydrophobic and aromatic residues and, to a lesser extent, polar residues.

Europe PMC Funders Author Manuscripts

Europe PMC Funders Author Manuscripts